DEVELOPING AN INDUCIBLE OSTEOCLAST SYSTEM AS A CELL THERAPY FOR ECTOPIC CALCIFICATION

Cameron William Rementer

A dissertation

submitted in partial fulfillment of the

requirements for the degree of

Doctor of Philosophy

University of Washington

2017

Reading Committee:

Cecilia Giachelli, Chair

Marta Scatena

Ted Gross

Program Authorized to Offer Degree:

Bioengineering

Abstract

DEVELOPING AN INDUCIBLE OSTEOCLAST SYSTEM AS A CELL THERAPY FOR ECTOPIC CALCIFICATION

Cameron Rementer

Chair of the Supervisory Committee:

Cecilia Giachelli, Department of Bioengineering

Ectopic calcification (EC) is a complex disease in which mineral develops in abnormal locations. It can develop in a variety of locations throughout the body, including the vasculature, heart valves, and in orthopedic settings where it is more commonly referred to as heterotopic ossification (HO). Current therapies for these conditions are limited and new treatment modalities would benefit a wide variety of patients. Osteoclasts resorb mineral *in vivo* and we hypothesized that a cell therapy based on inducible osteoclast differentiation could be used as a cell therapy to treat EC and HO.

The RANK/RANKL pathway is a critical step in osteoclast differentiation and we created an inducible RANK (iRANK) fusion protein which could be activated by a small molecule chemical inducer of dimerization (CID). This fusion protein was introduced into a macrophage cell line, and the resulting RAW264.7+iRANK cells were characterized using *in vitro* assays. In the presence of CID, the cells formed large, multinucleated, tartrate-resistant acid phosphatase (TRAP)-positive cells capable of resorbing two-dimensional mineral substrates. We then

developed three-dimensional assays that were used to test the capabilities of our cell line, including mineralized fibrin scaffolds, murine calvarial discs, and samples of human HO. These cells were capable of resorbing existing mineral, but also of preventing further mineralization of the human HO samples in a contact-independent manner. Finally, we characterized the behavior of RAW264.7+iRANK cells *in vivo.* We labeled and tracked the cells using bioluminescence and developed a collagen cell delivery vehicle to retain cells at the injection site. The cells were introduced into a murine model of HO where bone morphogenic protein 2 (BMP-2) is injected into the calf muscle to induce formation of an HO lesion. Using microcomputed tomography to quantify the volume of the HO over time, we found that in mice treated with RAW264.7+iRANK cells, there was a significant decrease in HO volume compared to baseline over a two week period, whereas in mice which did not receive cells there was no significant change over this period. Histological examination allowed us to locate the HO lesion and GFP-positive cells in close proximity. This research represents a novel approach to the treatment of EC and the *in vitro* study of osteoclastogenesis using the RAW264.7+iRANK cell line, and also the three-dimensional mineral assays.

TABLE OF CONTENTS

LIST OF FIGURES

LIST OF ABBREVIATIONS

BME	basement membrane extract
BMP-2	bone morphogenic protein 2
CAVD	calcific aortic valve disease
CID	chemical inducer of dimerization
EC	ectopic calcification
EDTA	ethylenediaminetetraacetic acid
ESRD	end stage renal disease
FBS	fetal bovine serum
GFP	green fluorescent protein
H&E	hematoxylin and eosin
HO	heterotopic ossification
iPSC	induced pluripotent stem cell
iRANK	inducible receptor activator of NFKB
LPS	lipopolysaccharide
M-CSF	macrophage-colony stimulating factor
microCT	microcomputed tomography
MuNC	multinucleated cell
OPN	osteopontin
OPG	osteoprotegrin
PBS	phosphate buffered saline
PMMA	polymethylmethacrylate
RANK	receptor activator of NFKB
RANKL	receptor activator of NFKB ligand

TRAP tartrate resistant acid phosphatase

VC vascular calcification

ACKNOWLEDGEMENTS

I would like to thank Meiting Wu who got me started on this project in the Giachelli lab and taught me so many techniques as well as giving me the most important advice I've received about working in research – "Be brave." Additionally, Mandy Lund and Worakanya Buranaphatthana collaborated endlessly with me to advance our therapeutic approach. The *in vivo* experiments would not have been possible without the contributions of Steve Bain, Brandon Ausk, and Dewayne Threet. I also received a great deal of assistance with a variety of techniques from Liz Soberg, Mary Wallingford, and Melissa Jackson. Finally, I must thank all of my committee members for their advice and guidance, especially Cecilia Giachelli and Marta Scatena.

DEDICATION

I dedicate this dissertation to my parents, brother, and friends. I would not be where I am without you and I am so grateful for that. To my parents, I want to thank you for working endlessly to help me develop intellectually and supporting me in so many ways. To my brother, you are my best friend in the world and going through the grind of grad school was made easier by the fact that we've been in the same boat for the past 4 years. To all of my friends, you have been a steady source of encouragement, empathy, and escape and have made the journey all worthwhile.

CHAPTER 1

Introduction

1.1 Significance and Innovation

1.1.1 Ectopic calcification

Ectopic calcification (EC) is a disorder which soft tissue becomes abnormally mineralized. This mineralization has many similarities to bone, and can occur as a result of injury, disease, and aging [1]. Heart valves are prone to calcification, which is known as calcific aortic valve disease (CAVD). CAVD is common in the elderly, and affects over 2% of people 65 years of age and older [2]. Risk factors for developing CAVD are age, hypertension, hypercholesterolemia, and diabetes, making CAVD a growing problem [3]. It is associated with a variety of negative health outcomes, including increased risk of congestive heart failure and cardiovascular death [4]. Vascular calcification (VC) is frequently observed in atherosclerotic lesions, and is particularly common in patients with end stage renal disease (ESRD) and diabetes. These patients are at heightened risk of myocardial infarction and stroke [5]. In orthopedic settings, abnormal calcification is usually referred to as heterotopic ossification (HO) and is associated with joint injury, burns, and brain/spinal injury [6]. HO is currently thought to result due to the osteogenic cytokine milieu that is present near sites of injury [7]. It is a growing problem, especially for veterans injured in combat. One study found up to 82% of soldiers developed HO if they had a spinal cord injury after being wounded by an improvised explosive device [8]. HO often results in pain, immobility, and decreased quality of life.

1.1.2 Current treatments

Treatments for the various forms of EC are lacking. The current method of treating CAVD is replacement of the diseased valve with a bioprosthetic valve. However, calcification remains the major mode of failure for these valves making valve replacement a temporary solution [9]. In patients with ESRD, various drug therapies are used to slow the progression of VC, including phosphate binders and calcimimetics, but they have limited efficacy thus far [10]. Other approved drugs, including bisphosphonates and statins, have been tested in humans but so far have shown limited benefits. Human trials of statins found no effect on valve calcification and human trials of bisphosphonates have had conflicting results. The major modes of treating HO occurring around joints and bone are surgical removal and radiation therapy. Surgical removal is complicated by the abnormal formation of HO which may include neurovascular entrapment [11]. Radiation therapy has some level of efficacy in preventing HO formation after joint replacement, but the treatment must be timed to coincide with the surgery, making it unsuitable for patients with HO from trauma, or for those who have established HO [12].

1.1.3 Innovation

We used a chemical inducer of dimerization (CID) system based upon the trimerization of an engineered surface receptor; previous studies have only examined dimerization with this system, which is insufficient for osteoclastogenesis [13]. This allowed us to control the differentiation of an engineered cell line into functional osteoclasts. We also developed and characterized a variety of novel three-dimensional models of EC for testing the resorptive capabilities of our engineered cells. The models we developed have important applications in studying osteoclastogenesis, an area of intense research. Additionally, the models could expedite research into therapies for EC,

as the systems we will develop are more physiologically relevant than existing *in vitro* models, but take less time to conduct than current *in vivo* models. Finally, we performed the first *in vivo* experiments studying the effect of our engineered cell line on a murine model of HO.

1.2 Background

1.2.1 Osteoclast biology

Osteoclasts are the cells responsible for bone resorption and differentiate from precursor cells of the myeloid lineage [14]. The mechanisms regulating osteoclast differentiation from monocytic precursors have been extensively studied. Two key cytokines, macrophage colony-stimulating factor (m-CSF) and receptor activator of NF-κB ligand (RANKL) are necessary and sufficient for osteoclast differentiation and activation. M-CSF induces monocytic precursors in bone marrow to proliferate and the binding of RANKL to its receptor, RANK, drives osteoclast differentiation, fusion, activation and survival. Osteoblasts trigger this process by producing RANKL and M-CSF. RANK is a type I transmembrane protein originally cloned from dendritic cells [15]. RANK belongs to the tumor necrosis factor receptor superfamily and assembles into functional trimers upon ligand binding. Trimerization triggers downstream NF-κB, MAPK and phosphatidylinositol signaling required for osteoclast differentiation [16-17]. Osteoprotegerin (OPG) is a potent inhibitor of osteoclast differentiation and survival by acting as a decoy receptor for RANKL [14]. Together, M-CSF and the RANK/RANKL/OPG axis act as major regulators of osteoclast formation and function in the bone (Fig 1.1).

1.2.2 Osteoclasts in ectopic calcification

At sites of EC, bone-forming cells are frequently observed, but osteoclasts are found infrequently, if at all. One study of explanted calcified valves found less than 4% of the valves had osteoclasts present, despite the fact that RANKL and M-CSF are present at sites of CAVD [18-20]. The low levels of osteoclasts seen in VC and CAVD calcification may be explained by the high levels of OPG found at these sites, which is associated with an inhibition of vascular calcification. We hypothesize that the development of EC could be prevented or reversed by a cell therapy using osteoclasts.

1.2.3 Cell therapy using osteoclasts

Cell therapy using osteoclasts, which resorb bone, has been proposed as a method for preventing or regressing mineral in a few preliminary studies, but so far no group has pursued this approach past the *in vitro* stage [21]. This is likely due to the difficulty of delivering osteoclasts, which are large multinucleated adherent cells. They are fragile and difficult to manipulate in culture, and are also terminally differentiated cells with a limited lifespan of about 2 weeks [22-23]. Our approach avoids the problems with using pre-differentiated osteoclasts by using precursors that can be induced to form osteoclasts after delivery.

1.2.4 Chemical inducer of dimerization system

This system is based on the chemical inducer of dimerization (CID) technology that has been used extensively to regulate growth and apoptosis of genetically modified cells [24-28]. The system generally consists of an intracellular receptor signaling domain linked to a fusion protein (FKBP12) that provides a binding site for a drug called CID [29-31]. Since RANK requires

trimerization for effective signaling [14], we have engineeered two FKBP12 domains fused to the RANK cytoplasmic domain to ensure successful oligomerization (Fig. 1.2A). Our data demonstrate that trimerization/oligomerization of engineered RANK recepter generates fully functional osteoclasts from monocytic precursors. To the best of our knowledge, this is the first use of CID technology to control any type of cellular differentiation, and may be used in the future to develop osteoclast cell therapies or high throughput testing systems for drug discovery.

1.2.5 Therapeutic approach

Figure 1.2B outlines our proposed therapy, which would involve first obtaining autologous precursor cells from the patient or using induced pluripotent stem cells (iPSCs) from the patient or a cell bank. These cells would be engineered to express the iRANK receptor, after which they would be delivered locally or systemically depending on the location of the EC being treated. Then CID would be delivered to induce osteoclast formation and mineral resorption.

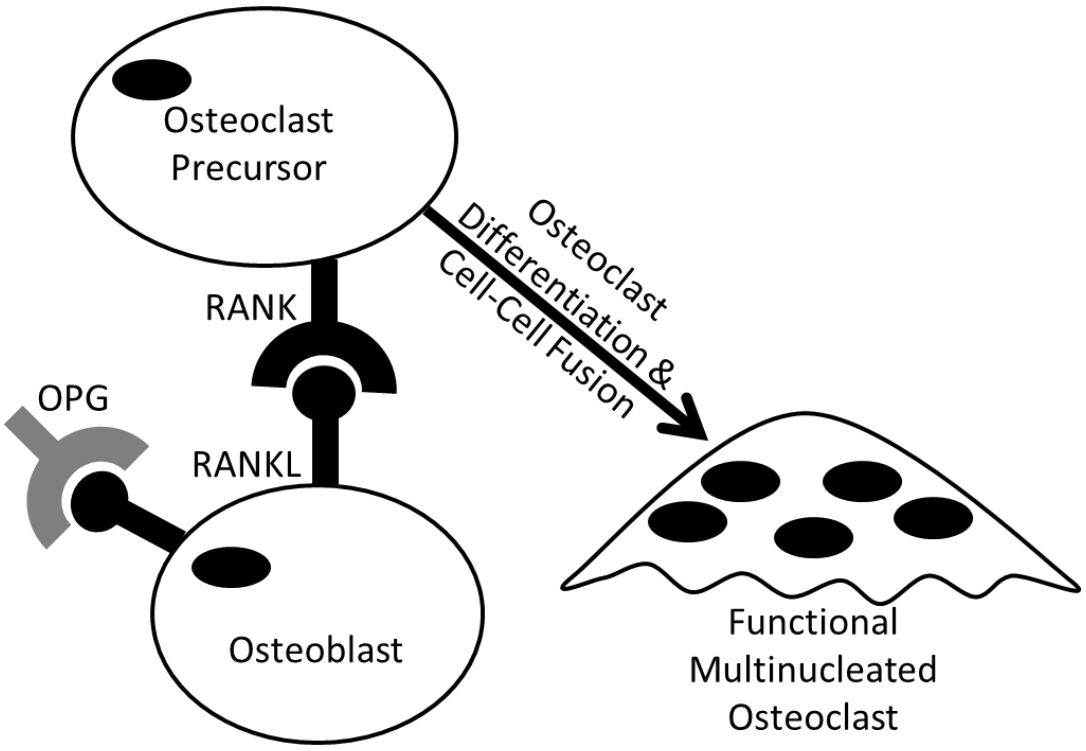

Figure 1.1: Schematic representation of the RANK/RANKL/OPG signaling pathway. Osteoblasts express RANKL on their surface which binds to RANK on osteoclast precursors. This initiates the differentiation and cell-cell fusion process that results in multinucleated osteoclasts capable of resorbing bone. OPG is a decoy receptor also capable of binding RANKL, thus inhibiting osteoclast formation.

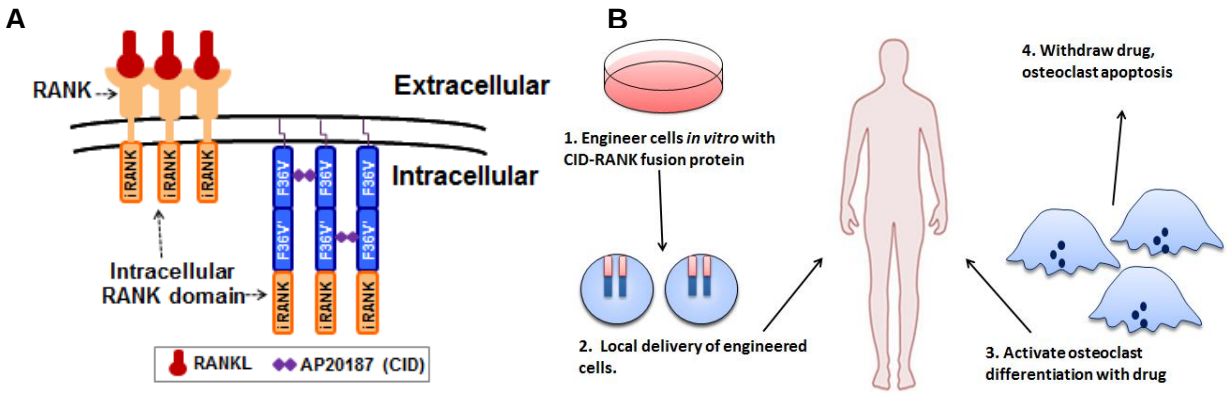

Figure 1.2: Experimental approach. (A) RANK signaling is initiated by trimerization of the RANK receptor in the presence of RANKL. The fusion protein consists of the cytoplasmic RANK domain linked to two F36V binding sites, which allows for trimerization of the protein in the presence of the CID, AP20187. (B) Cell therapy for EC could consist of engineering autologous precursor cells or iPSCs *in vitro t*o contain an iRANK receptor and then delivering the cells locally or systemically and activating osteoclastogenesis with CID. After treatment, cells undergo apoptosis either due to reaching the end of their limited lifespan or withdrawal of CID. (Credit: Mandy Lund)

CHAPTER 2

Characterizing RAW264.7+iRANK cells *in vitro*

2.1 Abstract

In this chapter, we investigated the ability of our engineered cell line, RAW264.7+iRANK cells, to differentiate into osteoclasts and resorb mineral. Osteoclasts are bone-resorbing cells that are critical for the normal formation and maintenance of teeth and skeleton. Osteoclast deficiency can contribute to EC, a pathology that is particularly detrimental to the mechanical functions of joints, valves and blood vessels. A reliable method for controlled generation of osteoclasts would be useful as a potential cell therapy for EC, as well as high-throughput drug screening for anti-osteoporotic drugs. Trimerization of RANK is known to be essential for osteoclast differentiation from monocyte/macrophage precursors. We previously engineered a murine monocytic cell line, RAW264.7, to express a fusion protein comprising of the intracellular RANK signaling domain and FK506-derived dimerization domains that bind to a small molecule CID. RAW264.7+iRANK cells treated with CID showed dose-dependent induction of tartrate-resistant acid phosphatase activity, as well as multinucleated osteoclast formation. Furthermore, NF-κB signaling was upregulated in a CID-dependent fashion, demonstrating effective RANK intracellular signaling. Functionally, CID-induced osteoclasts had robust mineral resorptive activity in a two-dimensional *in vitro* resorption assay. Most importantly, the engineered cells differentiated into osteoclasts that were resistant to the potent osteoclast inhibitor, osteoprotegerin. These studies are the first to describe a method for inducible control of monocytic precursor differentiation to osteoclasts, which could be used for the development of an engineered autologous cell therapy.

2.2 Introduction

In the following studies, we characterized a novel bioengineered system for conditional regulation of osteoclast differentiation from monocytic precursors. This system is based on the CID technology that has been developed to control cell proliferation and apoptosis [24-31]. Our data demonstrate that the iRANK receptor is able to generate fully functional osteoclasts from monocytic precursors in the presence of CID. These osteoclasts form even in the presence of OPG, an inhibitor of osteoclast differentiation. To the best of our knowledge, this is the first use of CID technology to control any type of cellular differentiation, and may be used in the future to develop osteoclast cell therapies or high throughput testing systems for drug discovery.

2.2.1 Current methods of osteoclast production

The gold standard for creating functional osteoclasts *in vitro* involves culturing osteoclast precursor cells in the presence of cytokines. If primary osteoclasts are required, monocytes from bone marrow or human peripheral blood is cultured in the presence of two cytokines, macrophage colony stimulating factor (m-CSF) and receptor activator of nuclear factor-κB ligand (RANKL) [32-33]. A more common method involves culturing RAW264.7 mouse macrophages in the presence of RANKL alone. These cytokines are expensive and have a very short half-life in solution. Once osteoclasts have formed they can be identified as multinucleated cells that stain positive for tartrate resistant acid phosphatase (TRAP).

2.2.2 Inducible differentiation of osteoclasts

Our lab has previously created a cell line possessing a gene for an inducible RANK receptor. The CID system is based upon linking the desired intracellular receptor signaling domain to a protein

(FKBP12) with a binding site for the CID. In the presence of CID, the fusion protein will dimerize. Our iRANK receptor possesses two binding sites (F36V and F36V') to allow for the trimerization necessary for RANK signaling. We developed the iRANK receptor to overcome the many limitations of using pre-differentiated osteoclasts, including their large size, fragility, and short lifespan. Using a lentiviral vector, RAW264.7 cells were transduced with the iRANK receptor. The construct also contained the gene for green fluorescent protein (GFP), which allowed for cell sorting to be performed. Cells were sorted twice by FACS to obtained a purified (>98% GFP+) population for *in vitro* characterization [34].

2.3 Materials and Methods

2.3.1 Cell culture

RAW264.7 cells were obtained from ATCC (Manassas, VA). Cells were cultured in D-MEM media from Invitrogen (Carlsbad, CA) containing 10% (v/v) heat-inactivated FBS and 100 U/ml pen/strep (Invitrogen) and incubated at 37°C with 5% CO2.

2.3.2 TRAP activity assay

Ten thousand cells were plated in 48-well plates and treated with RANKL (40 ng/ml), 0.1% ethanol (EtOH) or varying concentrations of AP20187 (ARIAD Pharmaceutics, Cambridge, MA). Supplemented media was changed every 2 days for 4 days. Cells were washed twice with PBS and lysed at RT for 10 min with 60 µl lysis buffer containing 100 mM Na Acetate pH 5.2, 50 mM Na Tartrate pH 4.9 and 2% NP40. Forty µl of cell extract was combined with 40 µl of reaction buffer (lysis buffer with 2.5 mM N-ASBI-P) in a 96-well plate at 37°C for 30 min, and the reaction was stopped by the addition of 20 µl 0.5 M NaOH [35]. Fluorescence was measured

using a microplate reader Safire2 (Tecan Group Ltd, Switzerland) with an excitation wavelength of 405 nm and peak emission wavelength of 520 nm.

2.3.3 TRAP staining

Twenty thousand cells/well were plated in 4-well Lab-Tek™ chamber slides (Nalge Nunc International., Rochester, NY) and treated with vehicle control (0.1% EtOH), RANKL (40 ng/ml) or AP20187 (0.1-50 nM in 0.1% EtOH) for 4 days. Cells were washed twice with PBS, fixed with 10% buffered formalin for 5 min and subjected to tartrate resistant acid phosphatase (TRAP) staining (Sigma., St Louis, MO) following the manufacturer's instructions. Slides were mounted with Aqua-Mount and images were obtained using an upright microscope (Nikon E800).

2.3.4 NF-κB expression

NF-κB is the major signaling pathway activated by RANK in osteoclasts and the activity of NF-κB transcription factor is crucial for osteoclastogenesis [36-37]. RAW264.7+iRANK and RAW264.7 cells were treated with either lipopolysaccharide (LPS) (100 ng/ml), RANKL (40 ng/ml), or AP20187 (20 nM) and cells were harvested at 2 h, 4 h and 6 h. Luciferase activity was measured using a luciferase assay system (Promega Corp.) according to manufacturer's instructions and normalized using the Renilla.

2.3.5 Osteologic discs

RAW264.7+iRANK (2×10^3 cells/disc) cells were cultured on BD BioCoat Osteologic discs (BD Biosciences, Bedford, MA) in the presence of either RANKL (100 ng/ml) or AP20187 (100 nM) and the supplemented media was changed every 2 days for 10 days. The cells on the discs

were removed with 10% bleach. Discs were stained with von Kossa reagent following the manufacturer's instruction (BD Biosciences, Bedford, MA). Resorption pits were visualized using stereomicroscopy (Nikon SMZ1500) and quantified by image analysis.

2.3.6 Osteoclast survival study

Osteoclast formation could be observed after 4 days in culture and the number of osteoclasts began to decline after 1 week. RAW264.7+iRANK and RAW264.7 cells were cultured as previously described and treated with CID and RANKL, respectively. Cells were fixed after 4, 7 or 9 days and TRAP staining was performed before counting TRAP-positive multinucleated cells. In a parallel experiment, osteoclast formation was induced by either CID or RANKL for 4 days before removing the inducer and culturing for 0, 3, or 5 additional days and then fixing and TRAP staining the cells.

2.3.7 OPG inhibition study

RAW264.7 and RAW264.7+iRANK cells were plated at 1×10^4 cells/well in 48-well plates. Six hours after plating, cells were treated with the media containing either 1 nM RANKL or 10 nM AP20187 with increasing concentrations of OPG (RANKL or AP20187 to OPG at 1:1, 1:5 and 1:10 molar ratio). Cells were cultured for 5 days with media replaced once at day 3. Cells were then fixed and TRAP stained and imaged by light microscopy. Multinucleated TRAP-positive osteoclasts (with ≥ 3 nuclei) were quantitated.

2.3.8 Statistical Analysis

Results are expressed as mean ± SD unless otherwise specified. Significance between groups was determined by one-way ANOVA with Bonferroni's post-hoc test. p-values less than 0.05 were considered significant.

2.4 Results

2.4.1 TRAP activity increased with CID

To verify CID-responsiveness of the iRANK-transduced cells, RAW264.7+iRANK cells were treated with vehicle alone (EtOH), RANKL, or increasing concentrations of the CID, AP20187. RAW264.7+iRANK cells started to fuse and form multinucleated cells at day 3 with AP20187 treatment and the number of fused multinucleated cells increased with increasing concentrations of AP20187 (Fig. 2.1). Treatment of non-transduced RAW264.7 cells with RANKL induced osteoclast formation as expected, but no osteoclasts were observed in the presence of AP20187 at any concentration tested (data not shown). To confirm that the fused multinucleated cells were osteoclasts, TRAP activity, an important cytochemical marker of osteoclasts was examined. Both RAW264.7 and RAW264.7+iRANK cells were treated with either RANKL or AP20187 for 4 days and stained for TRAP. Robust TRAP-positive multinucleated osteoclast formation was observed in AP20187 treated RAW264.7+iRANK cells after four days, whereas untreated or vehicle (EtOH) treated RAW264.7+iRANK cells showed no osteoclast formation. Treatment of non-transduced RAW264.7 cells with RANKL induced TRAP-positive multinucleated cell formation as expected, but no TRAP-positive multinucleated cells were observed in the presence of AP20187 at any concentration tested (data not shown). Quantitatively, the number of TRAP-positive multinucleated cells induced with the lowest concentration of 1 nM AP20187 in

RAW264.7+iRANK was comparable to that induced by 40 ng/ml RANKL in RAW264.7 cells (Fig. 2.2A). Furthermore, TRAP activity in RAW267.4+iRANK cells was induced by AP20187 in a dose-dependent manner (Fig. 2.2B).

2.4.2 CID increased NF-κB expression

To examine NF-κB activation by AP20187, both RAW264.7 and RAW264.7+iRANK cells were transiently transfected with two plasmids, a luciferase reporter construct containing NF-κB sites derived from Igκ promoter driving the luciferase gene and a Renilla luciferase construct as the internal control. The transfected cells were then stimulated with either AP20187, RANKL, or LPS (a RANK independent NF-κB inducing agent) and luciferase activity was monitored after 2 and 4 h. The activation of NF-κB by AP20187 in RAW264.7+iRANK cells or by RANKL and LPS in RAW264.7 cells was observed as early as at 2 h after stimulation. At 4 h, AP20187-stimulated NF-κB activity in RAW264.7+iRANK cells (7.8 RLU/μg protein) was comparable to RANKL- (7.3 RLU/μg protein) and LPS- (6.7 RLU/μg of protein) stimulated NF-κB activity in RAW264.7 cells (Fig. 3). This result suggests that the transduced iRANK construct can mediate NF-κB signaling in response to AP20187 treatment in RAW264.7 cells.

2.4.3 RAW264.7+iRANK cells resorbed 2D mineral substrates

To quantify the two-dimensional mineral resorptive properties of AP20187-induced osteoclasts, RAW264.7+iRANK cells were cultured directly on Osteologic discs in the presence of either 100 ng/ml RANKL or 100 nM AP20187 for 10 days. Resorption pits were visualized using von Kossa staining and imaged using a stereo microscope (Fig. 2.4A). The images were analyzed using ImageJ and the resorption area was quantified as a percentage of the total disc area. The resorbed area in AP20187 treated RAW264.7+iRANK cells (~ 47%) was significantly higher

than the cells treated with RANKL alone (~7%) (Fig. 2.4B). This is likely due to the high levels of iRANK construct in the cells compared to endogenous RANK, since the cells were sorted to enrich for iRANK expressing cells.

2.4.4 Osteoclast survival study

The time course of accumulation of osteoclasts following continuous RANKL or CID treatment of RAW264.7 and RAW264.7+iRANK cells, respectively, is shown in Figure 2.5A. In RANKL-treated RAW264.7 cells, the number of osteoclasts increased with time and attained a maximum at day 7 followed by a large decline in osteoclast number by day 9. In contrast, CID-treated RAW264.7+iRANK cells achieved maximal osteoclast numbers by day 4, followed by large declines at days 7 and 9. These data suggested a limited life span of the differentiated osteoclasts even in the continued presence of inducing agent. To better examine the life span of RANKL or CID induced osteoclasts, a cell survival study following drug withdrawal from pre-formed osteoclasts was performed (Fig. 2.5B). RAW264.7 and RAW264.7+iRANK cells were treated with 40 ng/ml RANKL or 50 nM AP20187, respectively, for 4 days after which the drug was withdrawn (day 0) and the cells were cultured in media alone for another 3 or 5 days. The cells were fixed, TRAP stained, and multinucleated TRAP-positive osteoclasts were counted. At day 3 of drug withdrawal, the number of osteoclasts decreased to 44% of day 0 values in RAW264.7 cells and to 26% of day 0 values in RAW264.7+iRANK cells. By day 5 of drug withdrawal, there were only ~10% osteoclasts surviving in RAW264.7 cells and ~8% in RAW264.7+iRANK cells. These data suggest that regardless of inducing agent, the osteoclasts had a similar lifespan of about 5 days *in vitro.*

2.4.5 OPG did not inhibit osteoclast formation induced by CID

Finally, to determine if CID-induced osteoclasts were resistant to the osteoclast differentiation inhibitor OPG, RAW264.7+iRANK cells were treated with CID in the presence of increasing concentrations of OPG for 5 days. The total number of multinucleated TRAP-positive cells per well was unchanged even in the presence of the highest concentration of OPG (50 nM) (Fig. 2.6A). In contrast, RANKL-mediated osteoclastogenesis was completely inhibited by OPG even at the lowest concentration (0.5 nM) (Fig. 2.6B).

2.5 Discussion

The engineered RAW264.7+iRANK cells differentiated into TRAP positive, multinucleated osteoclasts in a dose dependent manner in response to CID treatment. Exposure to CID increased NF-κB expression and the engineered osteoclasts showed robust mineral resorptive activity on Osteologic discs. The CID-generated osteoclasts had a similar lifespan *in vitro* to RANKL-generated osteoclasts. Finally, CID-induced osteoclast differentiation occurred even in the presence of high concentrations of the natural RANK antagonist, OPG.

Although CID technology has been used as a proliferation or death switch for genetically engineering cells for over a decade, these studies are the first to successfully apply this technology to control monocyte differentiation to functional osteoclasts. A previous report attempted using only one dimerization domain fused to the cytoplasmic domain of RANK to induce RANK dimerization in the presence of CID [13]. However, use of this construct to induce simple dimerization of RANK failed to produce osteoclasts. In contrast, we utilized two dimerization domains fused to the cytoplasmic RANK receptor (iRANK fusion protein) that could allow for RANK trimerization or higher order oligomerization following CID binding. As

we have shown, our iRANK construct enabled cell differentiation into fully functional, multinucleated osteoclasts with greater bone resorption activity than RANKL-induced cells. In addition, the iRANK engineered cells differentiated into osteoclasts even in the presence of the potent osteoclast inhibitor, OPG. It is interesting to note that decreased responsiveness of the RAW264.7+iRANK cells to RANKL was observed in osteoclastogenesis assays. Since the iRANK construct was targeted to the plasma membrane by a myristoylation sequence, it is possible that overexpression of the iRANK fusion protein could lead to sequestration of factors required for downstream RANK signaling, such as TRAF6 or GAB2. Further experiments are necessary to test this hypothesis.

Our studies provide evidence of CID-controlled osteoclast formation from bioengineered monocytic precursors. One potential application for our system would be the treatment of abnormal calcium deposits using an autologous cell therapy. Bone marrow-derived osteoclasts were first reported to have the ability to reduce the mineral content in calcified aortic elastin without degrading the elastin matrix *in vitro*, and thus were suggested as a potential cell therapy for valve disease and other forms of ectopic calcification [21]. However, the idea of using autologous bone marrow-derived osteoclasts as a therapy for ectopic calcification is limited because of the presence of osteoclast inhibitors, like OPG. OPG is up-regulated early in disease progression in valve tissue [38] and in serum. The bioengineered system developed here could overcome this limitation, since osteoclast differentiation of precursors to osteoclasts is controlled by CID-regulated trimerization of the iRANK construct, and thus cannot be inhibited by OPG. Another limitation for using native osteoclasts induced by RANKL as therapy is that the precursor cells must be differentiated into osteoclasts *in vitro* prior to delivery as administering RANKL to initiate osteoclastogenesis, which is not feasible *in vivo*. Fully differentiated

osteoclasts are large and multinucleated which makes them fragile and difficult to deliver, making pre-differentiating osteoclasts for a cell therapy an unviable approach. Our system would allow for the activation of osteoclastogenesis *in vivo* by a small molecule CID. A cell therapy for treating abnormal calcification would involve first delivering mononuclear precursor cells to the desired site, followed by initiating the differentiation of osteoclasts *in situ* by the small molecule CID. This method would overcome the difficulties associated with delivering terminally differentiated osteoclasts to sites of abnormal calcification.

2.6 Limitations

In this chapter we characterized an inducible osteoclast system *in vitro*. A major limitation of these studies was the use of a macrophage cell line, RAW264.7 cells. Although this cell line is used extensively to study osteoclastogenesis, they are not primary cells. This makes them less physiologically relevant to the eventual application of this system and presented a number of challenges for the *in vitro* studies, as the cells would eventually overgrow the culture dish. This limited our ability to conduct longer *in vitro* studies. A second limitation was the limited analysis of osteoclast function, as we used a two-dimensional mineral assay, which lacks ECM proteins. EC and HO are complex three-dimensional tissues, possessing both mineral and matrix. The studies we conducted in Chapter 3 were performed to address this limitation.

2.7 Conclusions

In conclusion, we have engineered monocytic precursors to differentiate into osteoclasts under the control of the CID, AP20187. This differentiation does not require RANKL and M-CSF, and it is also resistant to inhibition by OPG. When combined with autologous precursors, this system could be used to develop a local cell-based therapy to treat or prevent ectopic calcification. In

addition, this system could be used to robustly and cost-efficiently generate osteoclasts for high throughput drug testing, and could facilitate discovery of new therapeutic agents against diseases of osteoclast over-activity that are independent of OPG. Having developed this system and characterized it *in vitro* in two-dimensional assays, we were able to move forward with this cell line to test the functional abilities of the engineered osteoclasts in three-dimensional assays as well as *in vivo*.

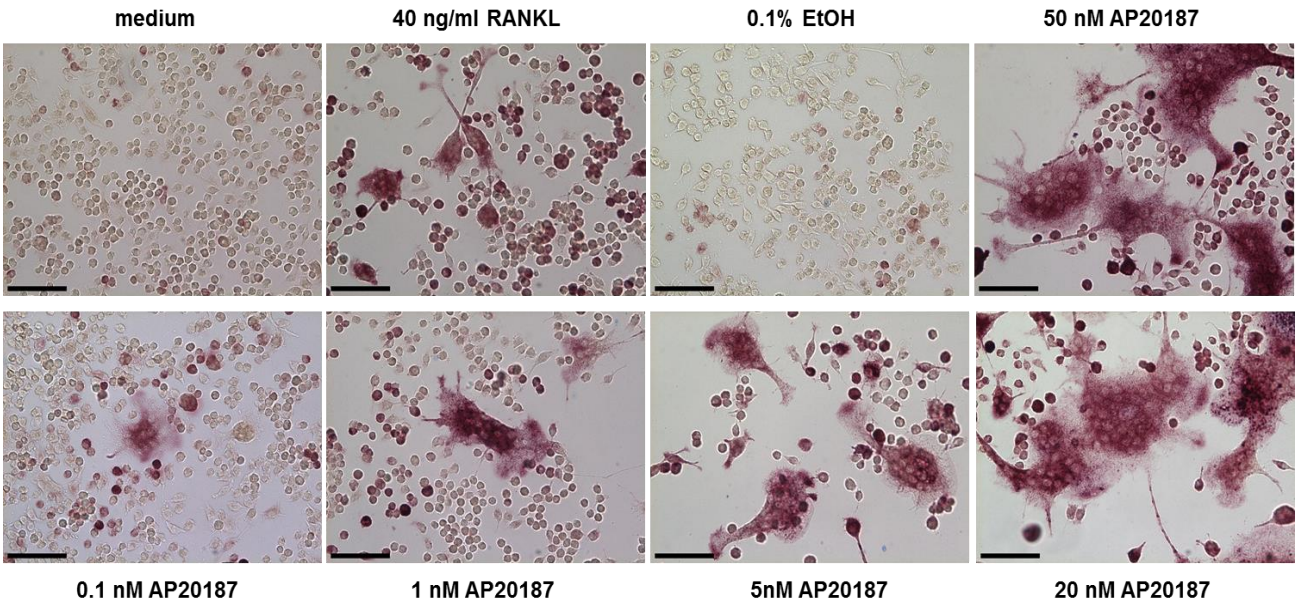

Figure 2.1: CID-responsiveness of the iRANK construct. RAW264.7+iRANK cells were cultured in media containing vehicle (EtOH), RANKL, or 0.1-50 nM AP20187 for 4 days and the cells were stained for TRAP. RANKL and AP20187 induced multinucleated TRAP-positive cells were observed (purple staining) (n = 3, scale bar = 100 µm).

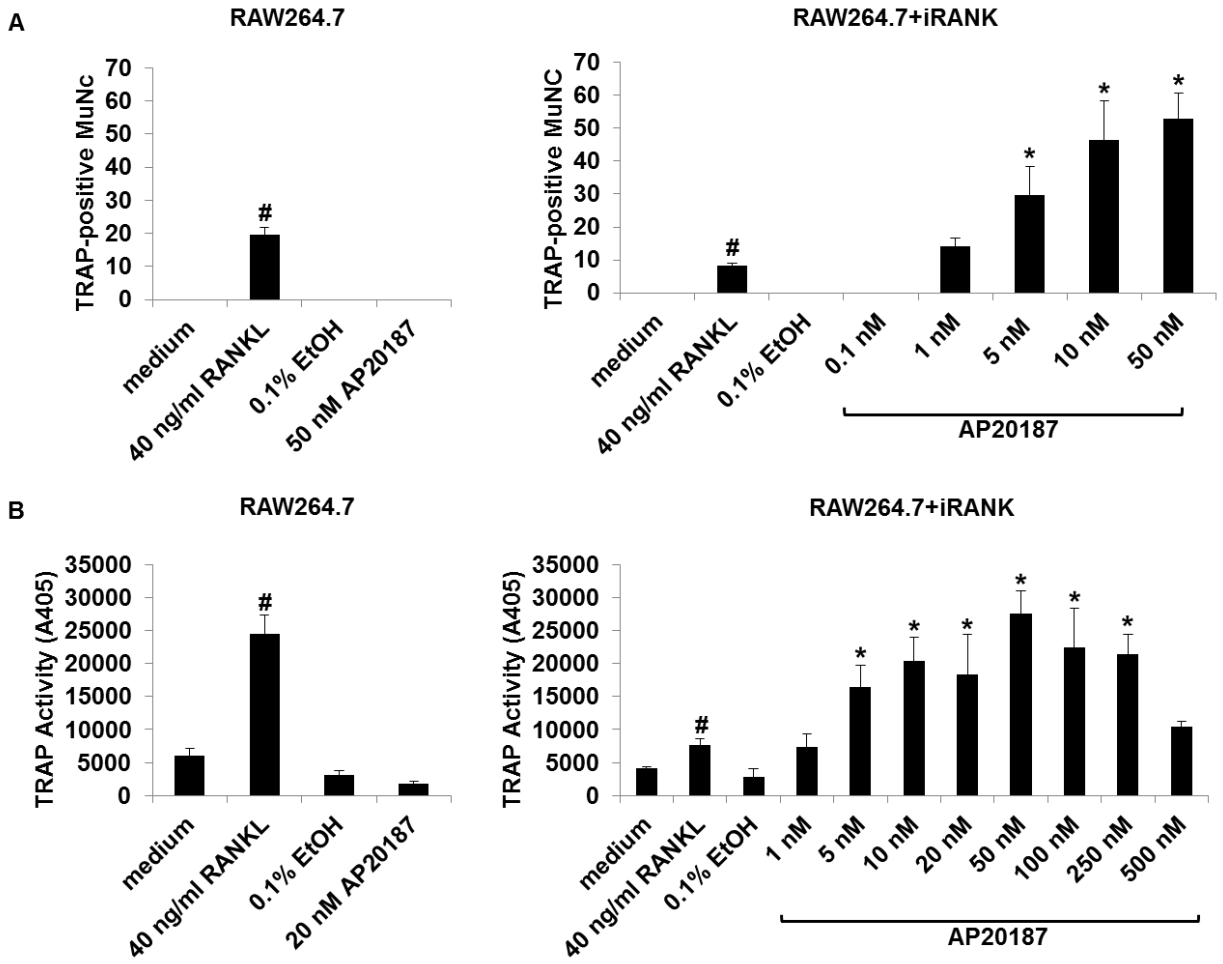

Figure 2.2: Dose-dependency of AP20187. (A) RAW264.7 and RAW264.7+iRANK cells were cultured in media alone, or media containing vehicle (EtOH), RANKL, or 0.1-50 nM AP20187 for 4 days and the cells were stained for TRAP. The number of TRAP-positive multinucleated cells (MuNC) was determined per 4 high power fields of view and averaged over 3 wells. Cells containing more than three nuclei were counted as multinucleated cells. (B) Dose-dependent induction of TRAP activity following RANKL or AP20187 treatment. Left panel: RAW264.7 cells. Right panel: RAW264.7+iRANK cells. n = 3 for all conditions. #$p<0.05$ compared to media, *$p<0.05$ compared to 0.1% EtOH.

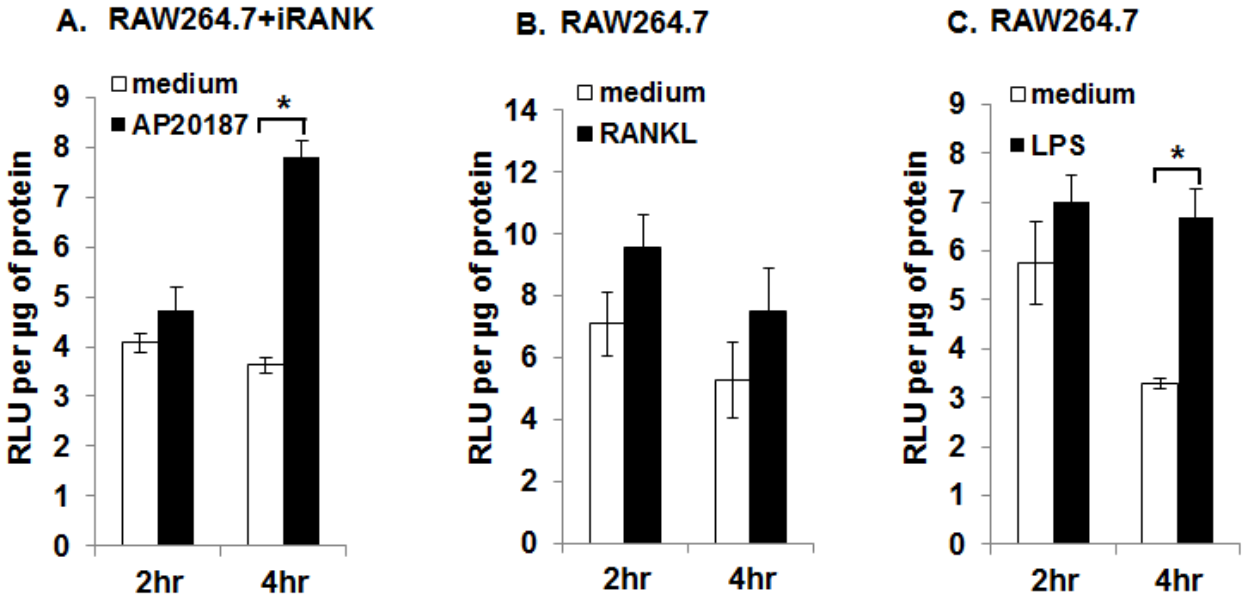

Figure 2.3: NF-κB dependent signaling in engineered osteoclasts. RAW264.7 and RAW264.7+iRANK cells were transiently transfected with a luciferase reporter construct containing NF-κB sites derived from Igκ promoter driving the luciferase gene and a Renilla luciferase construct as the internal control. NF-κB activation was measured in RAW264.7+iRANK cells stimulated with AP20187 (A), and RAW264.7 cells stimulated with RANKL (B) or LPS (C) for 2 and 4h. Data are average relative light units (RLU) per µg protein +/- SD with n = 4 for all conditions. *$p<0.05$.

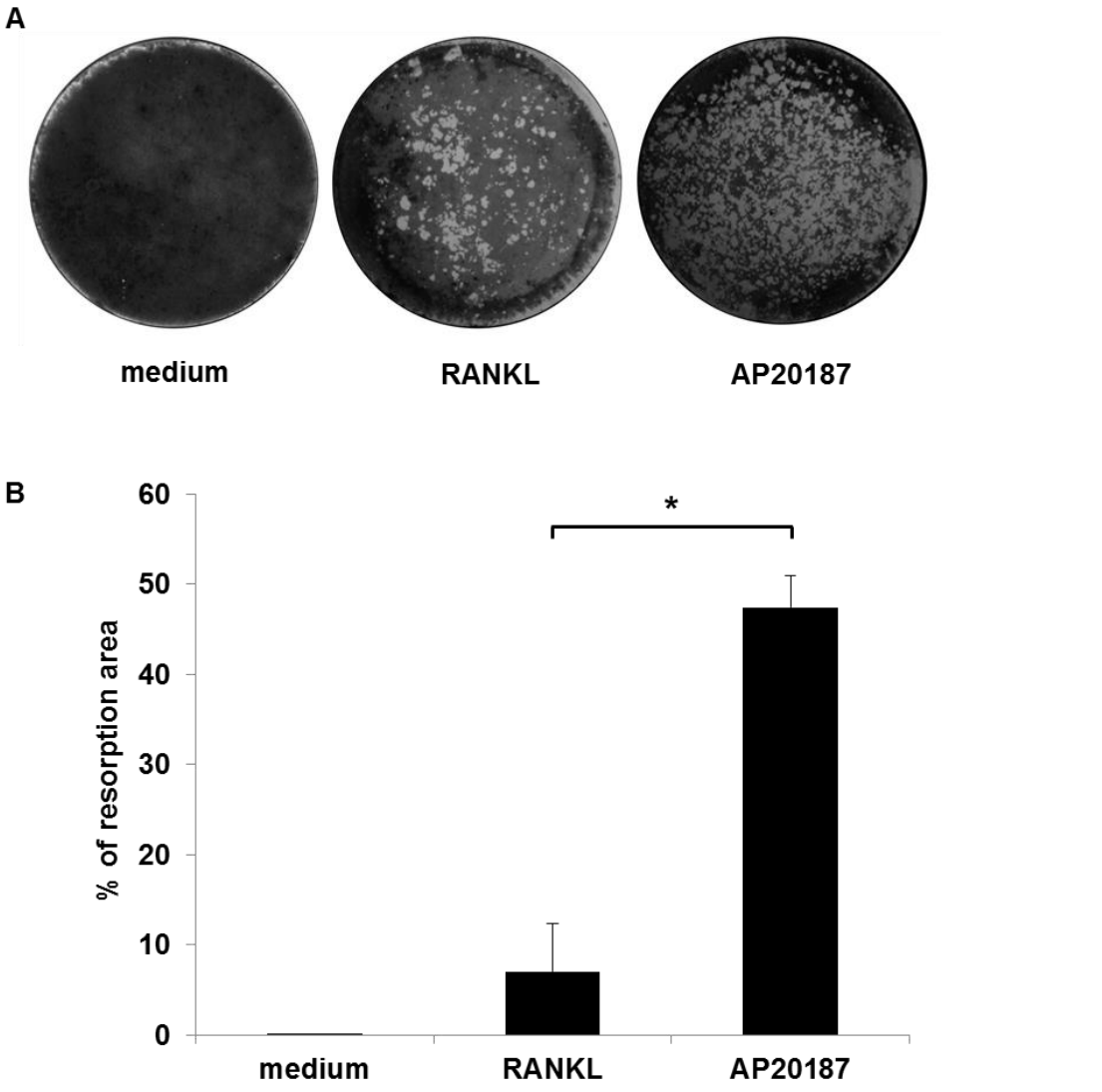

Figure 2.4: CID induced osteoclasts resorbed a two-dimensional mineralized substrate. (A) RAW264.7+iRANK cells were treated with either RANKL (100 ng/ml) or AP20187 (100 nM) on Osteologic discs. After 10 days, resorption lacunae were visualized by von Kossa staining. (B) The percent resorbed area per disc was measured and analyzed using ImageJ. Three experiments were averaged. Y-axis shows the % resorption per disc. n = 3 for all conditions. *$p<0.05$.

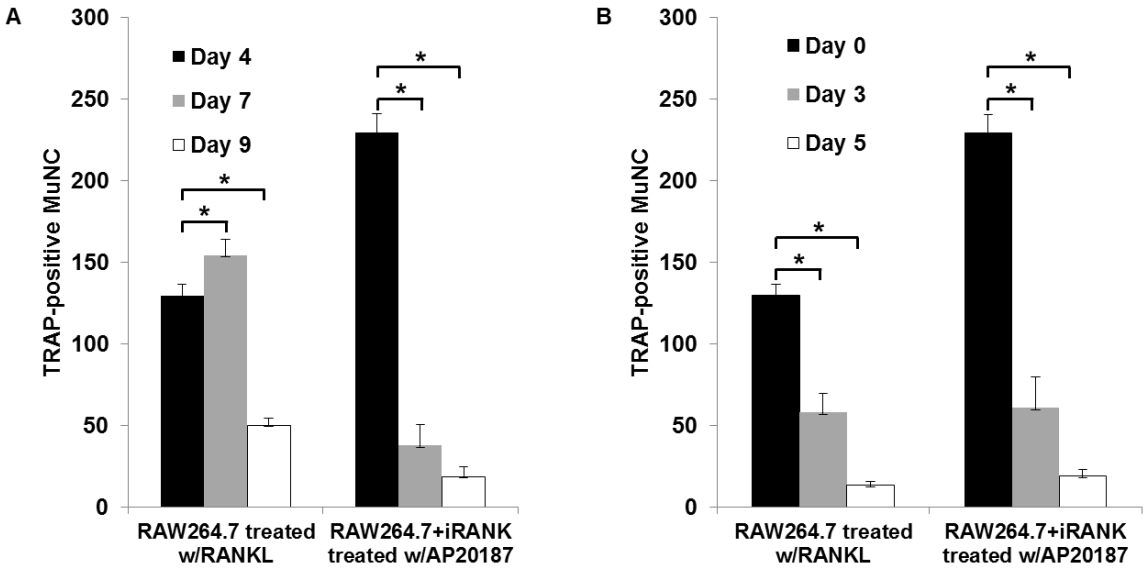

Figure 2.5: Cell survival study. RAW264.7 cells and RAW264.7+iRANK cells were treated with either RANKL (40 ng/ml) or CID (50 nM) for 4 days to allow osteoclasts to form. The supplemented media was removed, and cells were cultured for additional 0, 3 or 5 days in the presence (A) or absence (B) of inducers, and the number of TRAP-positive multinucleated cells (MuNC) per well was counted and averaged over 4 wells. n = 4 for all conditions. *$p<0.05$.

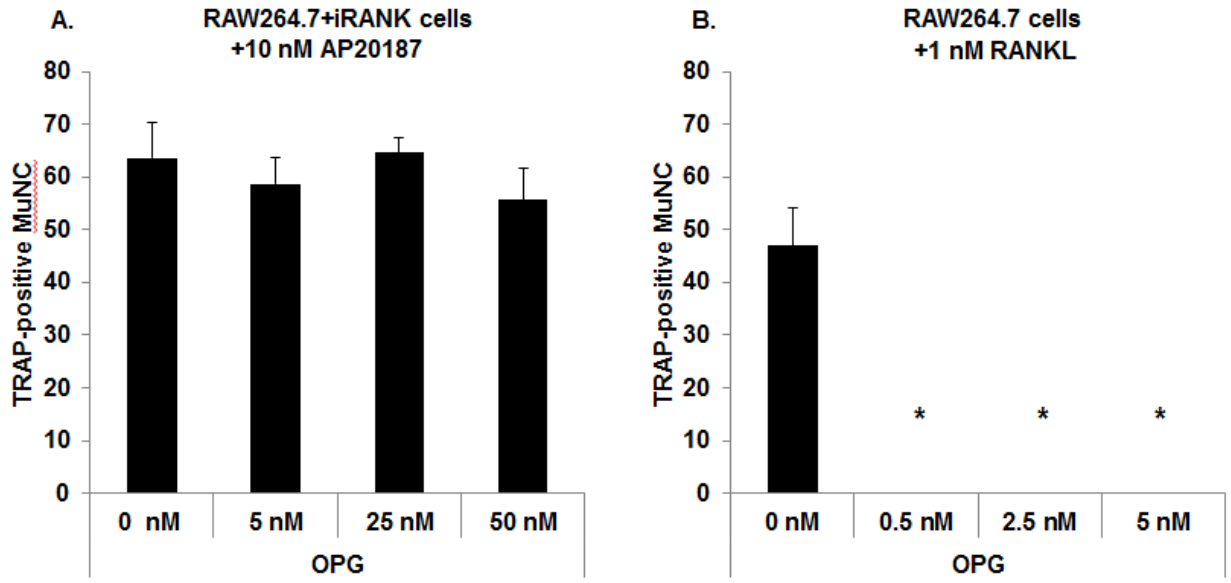

Figure 2.6: CID-induced osteoclastogenesis in RAW264.7+iRANK cells is not inhibited by OPG. TRAP-positive multinucleated cells (MuNC) after treatment of RAW264.7+iRANK cells with 10 nM AP20187 (A) or RAW264.7 cells with 1 nM RANKL (B) in the presence of increasing concentrations of OPG. TRAP-positive multinucleated cells (MuNC) were counted over 4 high power fields of view and averaged over 3 wells. *$p<0.05$ compared to 0 nM OPG.

CHAPTER 3

Three-dimensional *in vitro* models of heterotopic ossification

3.1 Abstract

In this chapter, the ability of RAW264.7+iRANK cells to resorb three-dimensional mineral *in vitro* was investigated. HO is the abnormal mineralization of tissue outside of the skeletal system. Cell therapy using osteoclasts has been proposed as a possible therapy for HO. Current methods for studying osteoclastic effects on mineralized tissues are lacking due to the fact that they rely on two-dimensional substrates and/or two-dimensional analysis, while HO is a three-dimensional tissue where mineral and matrix co-exist. In order to further verify the resorptive abilities of the inducible osteoclast system, we developed three-dimensional models of HO. The first we tested was mineralized fibrin scaffolds which were degraded more quickly by RAW264.7+iRANK cells. The second model we used was murine calvarial discs were generated and scanned by microcomputed tomography to measure mineral volume of the calvarial discs. After characterization, the discs were seeded with RAW264.7+iRANK cells. In the presence of CID, the discs decreased in volume compared to controls. Finally, samples of human HO were obtained from an orthopedic surgeon and were used to test the ability of the cell line to prevent mineral formation. These were found to grow in mineral content significantly less when cultured in conditioned media from RAW264.7+iRANK cells cultured with CID compared to controls. When the conditioned media was depleted of osteopontin (OPN), an inhibitor of mineral formation, they were found to increase significantly more. These models are novel and can be used to precisely quantitate the effects of engineered osteoclasts on mineral resorption and mineral growth of mineralized tissues.

3.2 Introduction

HO is a form of EC in which mature bone and marrow form after injuries, such as fractures and burns, as well as certain surgeries [39]. It has been increasingly reported in veterans injured by improvised explosive devices, which often result in both orthopedic injuries as well as severe burns [8]. In a study of 226 veterans who underwent amputations as a result of an IED explosion, HO was present in 55% of patients. These numbers were even higher for patients with a concurrent spine injury, with HO present in 82% [40]. The formation of HO can lead to debilitating consequences including immobility and severe pain due to neurovascular entrapment [11]. Treatment options are limited and the need for new methods of testing novel therapies is sorely needed.

3.2.1 Methods of measuring mineral resorption in vitro

In Chapter 2, we used Osteologic discs to measure mineral resorption by RAW264.7+iRANK cells. These are thin films of inorganic calcium phosphate and lack the matrix proteins and structure seen in HO. Other methods for quantifying mineral resorption *in vitro* exist but have various shortcomings. Dentin slices derived from human or animal teeth or bone slices can be cultured with osteoclasts and the formation of resorption pits can be quantified [41]. This method has both mineral and matrix, but the analysis often relies on two-dimensional histomorphometry. There are methods for measuring the volume of individual resorption pits using scanning electron microscopy or confocal microscopy, but these do not allow for the measurement of bulk effects on a substrate [42-43].

3.2.2 Novel in vitro models of HO

The search for treatments for EC and HO is hampered by the lack of relevant *in vitro* models which could accelerate research progress. A method that allows for the quantification of mineral growth and resorption in response to osteoclast treatment in three dimensions on a physiologically relevant substrate could provide a more accurate method for studying osteoclast activity. In this study, we present a method for quantifying osteoclastic mineral resorption and inhibition of passive mineral growth *in vitro* using microcomputed tomography (microCT). MicroCT is a non-destructive imaging modality that uses x-rays to create a 3D reconstruction of mineralized tissue [44]. Mineral resorption by engineered osteoclasts was measured on microporous mineralized fibrin scaffolds and murine calvarial discs, and the inhibition of passive mineral growth was measured on explanted samples of human HO. These models provide a quantitative method of studying different treatments for either the regression of stable HO or prevention of HO progression.

3.2.3 Role of osteopontin in mineralization

Osteopontin (OPN) is a potent inhibitor of mineralization *in vitro* and *in vivo*. Smooth muscle cells deficient in OPN will calcify *in vitro* [45]. Animal experiments have found that biomaterials implanted in OPN knockout mice will spontaneously calcify. This effect could be reduced by the delivery of exogenous OPN [46]. Our lab has promising research showing that the RAW264.7+iRANK cells are capable of preventing mineralization in a contact-independent manner, suggesting a soluble factor or factors are involved. For these reasons, we examined the effect of conditioned media on the human HO samples, with and without OPN depletion.

3.3 Materials and Methods

3.3.1 Cell culture and generation of osteoclasts

RAW264.7 cells were obtained from ATCC (Manassas, VA) and cultured in D-MEM media from Invitrogen (Carlsbad, CA) containing 10% (v/v) heat-inactivated FBS and 100 U/mL Pen/Strep (Invitrogen) and incubated at 37°C with 5% CO_2. Osteoclastogenesis was initiated in RAW264.7+iRANK cells by adding 50 nM AP20187 in this media.

3.3.2 Preparation of mineralized microporous fibrin scaffolds

Mineralized microporous fibrin scaffolds were prepared as previously described [47]. Briefly, polymethylmethacrylate (PMMA) beads were sintered at 174°C for 22 h before being infiltrated with a solution of fibrinogen and thrombin. After 16 h, the PMMA was dissolved away through acetone washes. Following this, the scaffolds were incubated with a physiological mineralizing solution for 48 h. These scaffolds were seeded with either RAW264.7+iRANK or RAW264.7 cells (2×10^4 cells/scaffold). The media was supplemented with AP20187 at 50 nM. At days 2, 5, 8 or 11 scaffolds were removed and weighed. They were then fixed in 10% formalin for 2 h before processing for histology. TRAP staining was performed using a commercial kit according to the manufacturer's instructions.

3.3.3 Preparation of calvarial discs

Murine calvarial discs were obtained from 4-5 week old wild-type C57BL/6 mice. After euthanizing the mice using carbon dioxide, an incision was made over the skull. The roof of the skull was excised with surgical scissors, and cleaned of adherent tissue using a sterile cotton swab. Two calvarial discs were obtained from each mouse using a 5 mm biopsy punch. These

were first rinsed in a solution of phosphate buffered saline (PBS) containing 1% antibiotic/antimycotic (a/a) twice. The calvarial discs were frozen in solution overnight to aid cell lysis. Each disc was placed in a vial containing 5 mL of 70% EtOH and then sonicated using a Tekmar Sonic Disruptor with amplitude set to 90 for 5 minutes twice. The discs were then rinsed in sterile water twice. Before scanning the discs by microCT, discs were dried in a Virtis Benchtop Lyophilizer overnight. The discs were also imaged using a Nikon digital camera.

3.3.4 Human HO model

Samples of human HO were obtained from a local orthopedic surgeon in the course of treatment. The human HO samples were stored in 70% ethanol before being sectioned into 600 μm slices using a Buehler low speed saw equipped with a diamond wafering blade. A biopsy punch was used to create 6 mm diameter discs. These were cleaned by sonication in 70% EtOH for 5 min 2X and then lyophilized.

3.3.5 Microcomputed tomography

High resolution microCT images of the samples were obtained using a Scanco VivaCt 40 (10.5 μm voxel size, 55 kVp, 145 μA) as previously described [48]. From these scans, the bone volume was calculated using a threshold of 250. Throughout the experiments, two calvarial discs were used as standards and were scanned with every batch, in order to ensure the accuracy of the other scans.

3.3.6 Acid decalcification of calvarial discs

To determine if microCT was an appropriate method for discerning mineral loss along a wide range of values for calvarial discs, we decalcified the samples for varying amounts of time. First,

discs were scanned by microCT as previously described to measure the starting bone volume. The discs were incubated in 5% hydrochloric acid for 5 s, 10 s, 30 s, 1 minute, 5 minutes, 15 minutes, 1 h, or 24 h. After this, the discs were rinsed 3X in PBS without calcium. Finally, the discs were lyophilized overnight and scanned as previously described to determine the final bone volume.

3.3.7 Cell seeding

After scanning the calvarial discs, they were cleaned again by rinsing in PBS containing 1% a/a, followed by 70% EtOH and finally ddH_2O. Discs were incubated in serum-containing media for 1 h prior to cell seeding. After 1 h, media was removed and the discs allowed to air dry for 10 minutes. Cells were seeded at $1x10^5$ per disc on the first side in 100 µL of media. The discs were placed in the incubator for 1 h to allow cell adhesion before seeding the second side. The discs were flipped into new wells and seeds with the same concentration of cells on the second side. These were allowed to incubate for 1 h further before replacing the media with either fresh media (negative control) or media containing the inducer, 50 nM AP20187.

3.3.8 Confocal microscopy

Confocal microscopy was used to image live RAW264.7+iRANK cells on calvarial discs. Just before imaging, Hoechst 33258 nuclear stain (Sigma-Aldrich, Inc.) was added to each well at a concentration of 1 µg/ml. A Zeiss 510 META Laser Scanning Microscope (LSM) was used to image the blue fluorescence from the Hoechst stain and GFP expression by the RAW264.7+iRANK cells. Images were processed using Zeiss LSM software.

3.3.9 Human HO

RAW264.7+iRANK cells were cultured in α-MEM containing 10% heat-inactivated FBS and 100 U/mL of penicillin/streptomycin and induced to differentiate into osteoclasts with 50 nM AP20187. Conditioned media was collected, centrifuged to remove cells and filtered through a 0.22 µM filter (Fisher Scientific, Hampton, NH). This was then mixed 1:1 with fresh media and incubated at 37°C with human HO samples and replaced daily for 5 days. Media from cells not exposed to CID was also used as a control. After 5 days, the samples were lyophilized and scanned by microCT as previously described.

3.3.10 Immunodepletion of Osteopontin in Conditioned Media

Dynabeads Protein G (1.5 mg) (Life Technologies, Carlsbad, CA) were incubated with OP-199 antibody (10 µg) for 30 min at RT on a rotator. Samples were placed within a magnet and bead-antibody complex was rinsed twice with PBS containing Tween-20. Conditioned media from CID-treated RAW264.7+iRANK cells bead-antibody complex and incubated for 1 h at RT on a rotator before placing the sample on the magnet. Conditioned media was finally transferred to a clean tube and filtered before adding to the human HO samples.

3.3.11 Statistical analysis

Significance between groups was determined by either one-way ANOVA with Bonferroni's post-hoc test (multiple groups) or T-Test (two groups) and p-values less than 0.05 were considered significant.

3.3.12 Ethics statement

Animal work was carried out to minimize animal discomfort by following the Guide for the Care and Use of Laboratory Animals of the National Institutes of Health. This work was approved by the University of Washington Institutional Animal Care and Use Committee (Protocol #2224-04). Human HO samples were obtained without our interaction with the patients and with no identifying information. Therefore, this research did not constitute human research although this was confirmed by the university.

3.4 Results

3.4.1 Mineralized fibrin scaffolds

Microporous fibrin scaffolds had a calcium content of 34.8±5.6 μg calcium/mg dry scaffold weight. We observed a significant decrease in the weights of the scaffolds seeded with the engineered osteoclasts compared to parental monocytes by day 11. Weight loss was minimal in scaffolds that did not receive cells at day 11 (Fig. 3.1A). When the scaffolds were examined by histology, multinucleated cells were observed by H&E staining within the scaffolds seeded with RAW264.7+iRANK cells, and all of these stained positively for TRAP (Fig. 3.1B), whereas no multinucleated TRAP-positive cells were seen in scaffolds seeded with RAW264.7 cells (data not shown).

3.4.2 Preparation and characterization of calvarial discs and human HO samples

Calvarial discs were prepared and imaged by digital camera (Fig. 3.2A) and microCT (Fig. 3.2B). First discs were excised from discarded C57BL/6 mice by removing the calvaria and then using a 5 mm biopsy punch to produce 2 discs from each mouse. These were cleaned by

sonicating in 70% ethanol twice. Overnight lyophilization was found to increase the reproducibility of discs on repeated scans. When discs were lyophilized prior to scanning, the coefficient of variation was found to be 0.007. Human HO samples were obtained from an orthopedic surgeon (Harborview Medical Center, Seattle, WA). These were transported in 70% ethanol and stored at -20°C until use. First, the HO samples were sectioned into 600 µm thick sliced using a Buehler low-speed saw with a diamond wafering blade. A 6 mm biopsy punch was used to obtain discs which were then cleaned by sonication in ethanol as previously described. These discs were lyophilized overnight before scanning by microCT.

3.4.3 MicroCT could detect a range of changes in mineral volume

To determine the useful range of mineral loss that could be measured by microCT, calvarial discs were decalcified in acid. Discs were scanned by microCT and partially demineralized in a dilute acid solution followed by repeat scanning and the smallest detectable mineral loss was 0.50% after 5 s and the largest mineral loss was 99.98% at 24 h (Fig. 3.3). This indicates that our method is useful for a wide range of mineral loss and can detect even small levels of mineral loss.

3.4.4 Osteoclasts were visualized on calvarial discs

RAW264.7+iRANK cells were cultured on murine calvarial discs and osteoclastogenesis was induced with CID. GFP-positive multinucleated cells were observed in the presence of CID (Fig. 3.4) but not in the absence of CID (data not shown).

3.4.5 Discs decreased in volume with RAW264.7+iRANK cells and CID

To determine the ability of engineered osteoclasts to resorb the calvarial discs, the discs were seeded with cells on both sides and treated with inducer. AP20187. The discs were found to lose mineral in an inducer-dependent fashion. Discs incubated in media alone grew more than 6.75% over the course of the experiment, while discs coated in cells grew by 0.85%. However, when discs coated in cells were treated with AP20187, the bone volume decreased significantly, by an average of -0.72% (Fig. 3.5).

3.4.6 Multiple cell seedings

To determine if the effects of the osteoclast activity were cumulative, calvarial discs were seeded with RAW264.7+iRANK cells multiple times. After 12 days, discs were cleaned and re-seeded with new cells. There was significant mineral loss at 12 days with one cell seeding (-1.77%) and at 22 days with two cell seedings (-3.84%). In contrast, discs seeded with cells and cultured without inducer showed 2.24% increase in mineral volume (Fig. 3.6).

3.4.7 Conditioned media from RAW264.7+iRANK cells inhibited mineral growth

Human HO samples were obtained after surgical explantation from an orthopedic surgeon. These samples grew in mineral volume over time in culture, simulating progression of HO *in vitro.* When incubated for 5 days in conditioned media from RAW264.7+iRANK cells the human HO discs also grew in volume. However, conditioned media from RAW264.7+iRANK cells cultured with CID inhibited this growth. The effect was lost by first depleting OPN from the conditioned media, suggesting OPN plays a role in the effect (Fig. 3.7).

3.5 Discussion

HO formation remains a difficult to treat medical condition in war-wounded veterans. The research to develop novel therapies could be accelerated by 3D *in vitro* models of HO, which would provide more physiologically relevant system. In this study, we have developed three 3D *in vitro* models of HO, mineralized microporous fibrin scaffolds, calvarial discs and human HO samples. We generated the fibrin scaffolds and found that their weight decreased more quickly when cultured with RAW264.7+iRANK cells in the presence of CID. For the calvarial discs, we characterized the reproducibility of microCT scans and the range of measurable changes in mineral volume. The effect of an engineered osteoclast cell line on mineral resorption was also examined in this system. We found that the discs decreased in mineral volume when seeded with cells in the presence of inducer. Finally, the effects of this cell line on mineral growth in human HO samples were investigated. Media from RAW264.7+iRANK cells cultured with CID inhibited mineral growth in a contact-independent manner. When this media was depleted of OPN, the effect disappeared, suggesting OPN plays a role in this inhibition.

The first question we investigated was whether mineralized microporous fibrin scaffolds could be used as an *in vitro* model of HO. These were previously developed as an approach to orthopedic tissue engineering. The scaffolds were generated using a sphere-templating technique and cultured with RAW264.7+iRANK cells. Although an effect on the dry weight of these scaffolds and we identified TRAP-positive cells within the scaffolds, these scaffolds were fragile and the macrophages were capable of breaking them down even without CID. This led us to pursue other *in vitro* models of HO.

Next, we tested murine calvarial discs, using microCT to measure changes in mineral volume. Our studies showing excellent reproducibility of scans and an extremely low limit of detection of mineral resorption led us to use these models in our studies of engineered osteoclasts. We demonstrated seeding both surfaces of the discs limited mineral growth. Many biomaterials undergo passive mineralization in physiological or supersaturated solutions [49-51]. RAW264.7 cells are known to express low levels of OPN, a potent inhibitor of calcification, *in vitro*, and this could help explain why we were able to ameliorate the mineral growth by dual cell seeding [52].

We then investigated was whether mineral resorption by engineered osteoclasts could be measured in calvarial discs by microCT. We found that discs cultured with the engineered cells and CID has a reduced volume which was significantly different from controls. One advantage of this model is it allows for the measurement of changes in a three-dimensional physiologically relevant sample. There are some commercially available mineral substrates consisting of a thin layer of inorganic crystalline calcium phosphate that can be used to quantify mineral resorption. However, these substrates are two-dimensional and most importantly, lack the matrix protein components of bone [53]. Another model used to study osteoclastogenesis is pit formation on human or animal dentin. This model possesses both mineral and matrix components, but the analysis is typically performed by 2D imaging of resorption pits, which does not fully capture what is occurring in the 3D microenvironment [54]. A second advantage of our system is that microcomputed tomography is a non-destructive method of measurement allowing for the examination of samples by other methods after scanning, or for using samples in multiple experiments with repeated measurements.

The final question we investigated was whether a model of developing HO, explanted samples of human HO, could be used to measure changes in mineral growth. We found that conditioned

media from RAW264.7+iRANK cells cultured with CID significantly inhibited passive mineral growth on the HO samples. Because this inhibition occurred in a contact-independent manner, we tried to determine what factors were mediating this effect. OPN is a potent inhibitor of mineralization [55-56]. We depleted the conditioned media of OPN and found that the inhibitory effect was lost. This suggests OPN plays a major role in the inhibitory effect, but further research is required to exclude the involvement of other anti-calcific factors.

3.6 Limitations

In this chapter we developed three-dimensional models for measuring the effect of RAW264.7+iRANK cells on mineral growth and resorption of existing mineral. One major limitation of these models is that they lack living cells. In EC and HO, there are a variety of cell types present, each having its own contribution to the prevention or promotion of mineral, and each interacting with the other cell types present. The fact that we used devitalized tissues means that the systems are less complex that the *in vivo* situation. Additionally, the lack of cells which promote mineralization means we are mainly examining the contribution of passive mineral growth to the development of EC/HO.

3.7 Conclusions

Available models for *in vitro* study of osteoclast resorption on three-dimensional substrates are limited and these methods may be useful for testing factors that inhibit or promote osteoclast function, or other potential cell therapies for HO. They may be generalized to measuring mineral resorption or inhibition in other samples. Taken together, these models could provide a useful means of accelerating current *in vitro* research in order to identify promising approaches to treating HO more rapidly. Additionally, by confirming that RAW264.7+iRANK cells could

resorb mineral and prevent its development in more physiologically relevant systems, we were able to proceed to the next stage of the study where we examined *in vivo* effects on a mouse model of HO.

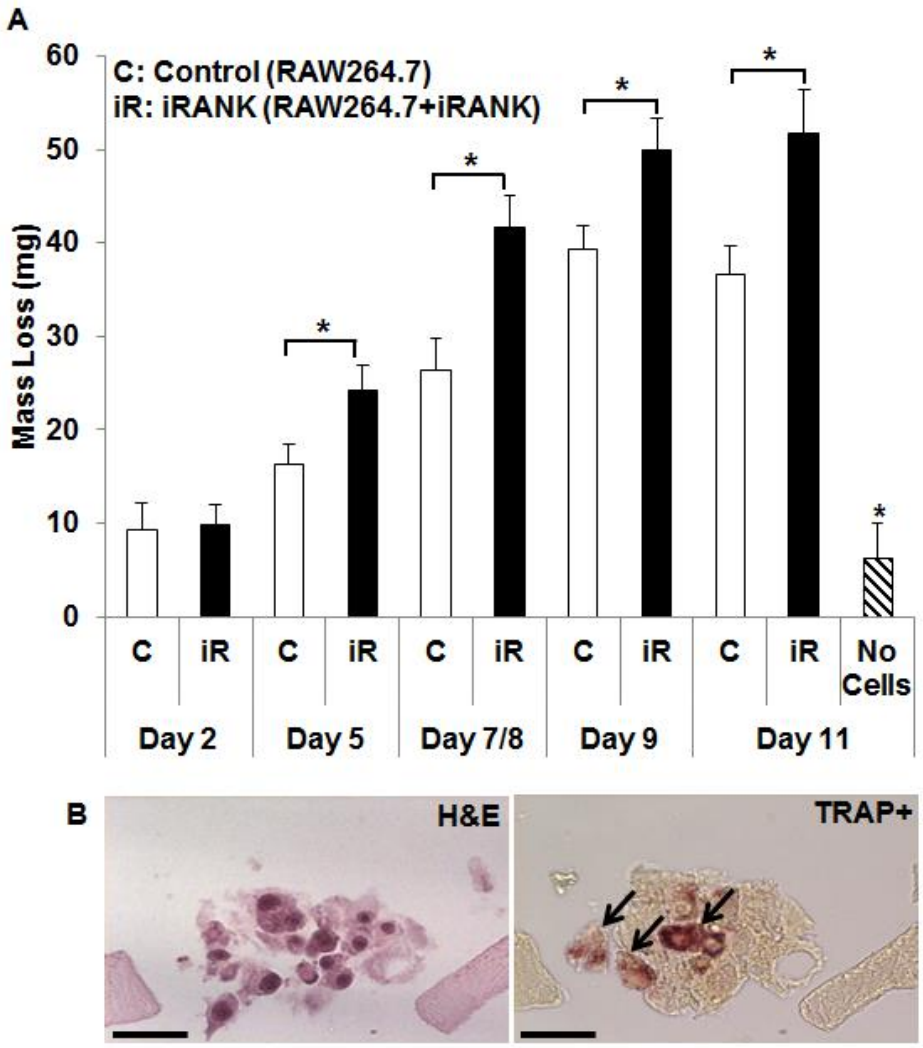

Figure 3.1: CID induced osteoclasts resorbed a three-dimensional mineralized substrate. (A) Mineralized fibrin scaffolds were seeded with control RAW264.7 cells (white bars) or iRANK transduced RAW264.7 cells (black bars), or no cells (hatched bar). The scaffolds were weighed at various time points (days 2, 5, 8 and 11). The scaffolds without cells were incubated in media for 11 days. Mass loss was calculated by subtracting the final mass from the initial mass. *p <0.05. (B) RAW264.7+iRANK were cultured with AP20187 in the fibrin scaffolds for 8 days. H&E staining (left panel) and adjacent TRAP staining (right panel) indicate the differentiation of osteoclasts within the scaffolds (arrows) n = 3 for all conditions. (scale bar = 50 μm).

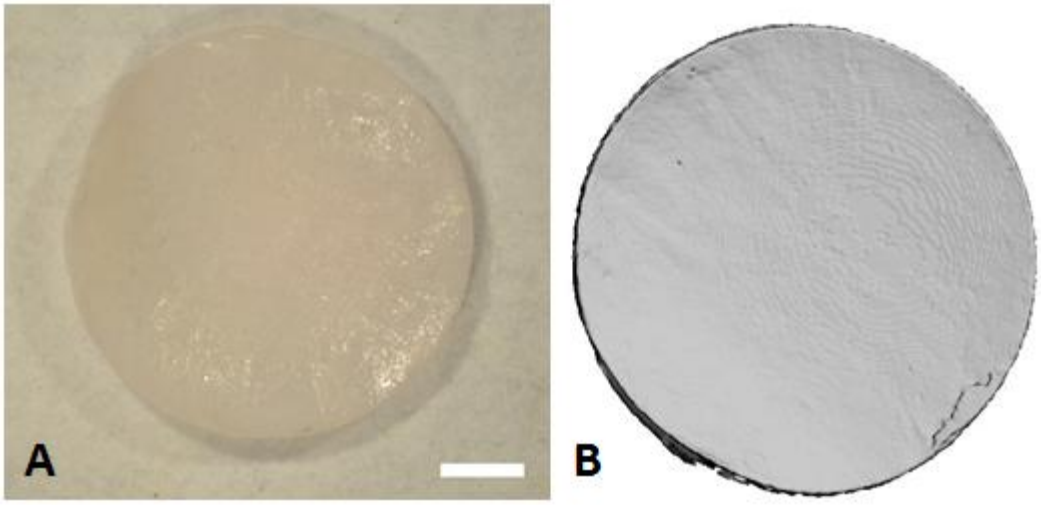

Figure 3.2: Calvarial discs were prepared and imaged. Calvarial discs were obtained from murine skulls with a 5 mm biopsy punch and cleaned by sonication. Images were obtained by digital camera (A) and by microcomputed tomography (B) (scale bar=100 μm).

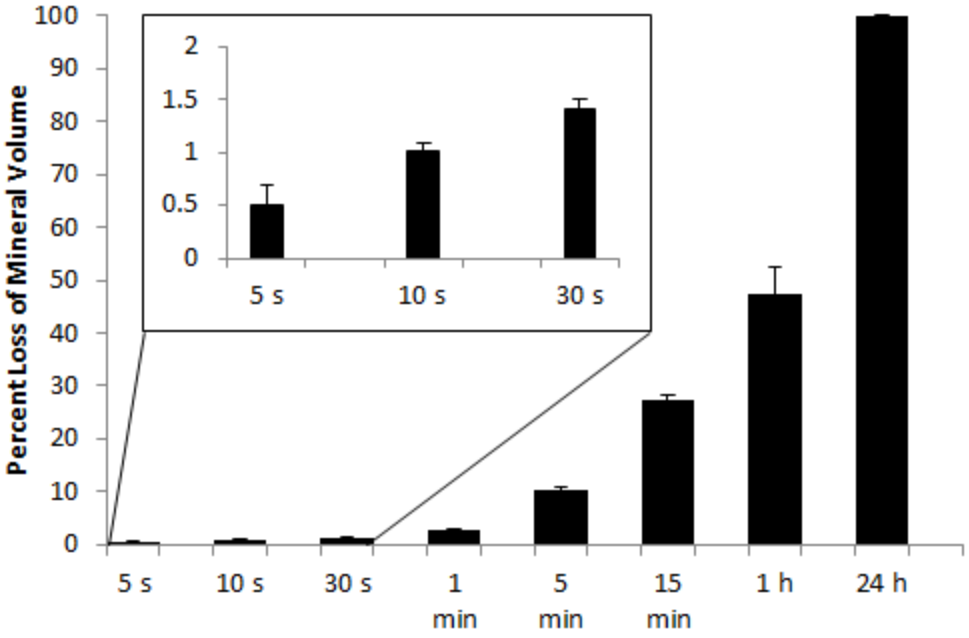

Figure 3.3: The range of measurable mineral volume loss was determined using acid decalcification. HCl was used to decalcify calvarial discs over 24 hours to determine the least and greatest amount of change and mineral volume. This method could measure large mineral volume changes with 99.87% loss at 24 h. Inset: Small changes could also be measured with 0.05% loss at 5 s. n = 2 for all conditions. Data are expressed as mean +/- SD.

.

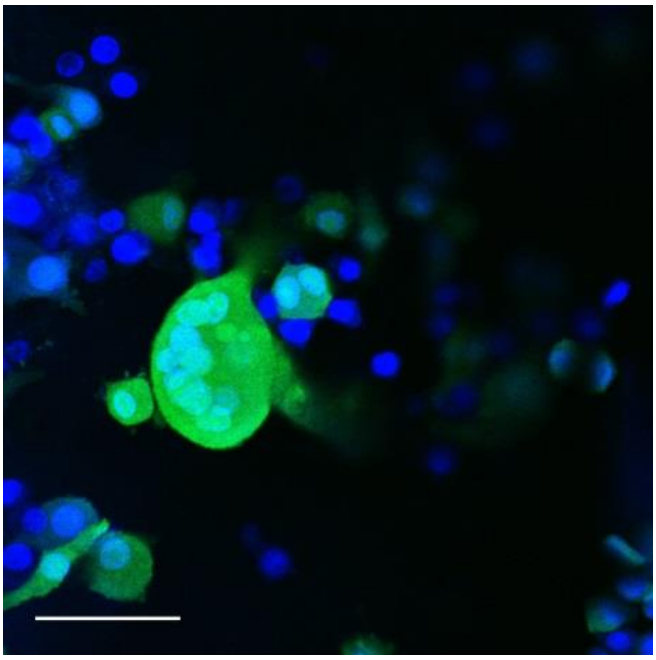

Figure 3.4: CID induced osteoclasts formed on calvarial discs. Confocal micrograph of multinucleated osteoclasts on a murine calvarial disc. Calvarial discs were seeded with RAW264.7+iRANK cells and osteoclast formation was induced by the addition of AP20187. Cells were imaged by confocal microscope; blue fluorescence indicates nuclei by Hoechst stain, while green fluorescence indicates GFP expression in RAW264.7+iRANK cells (scale bar = 50 μm).

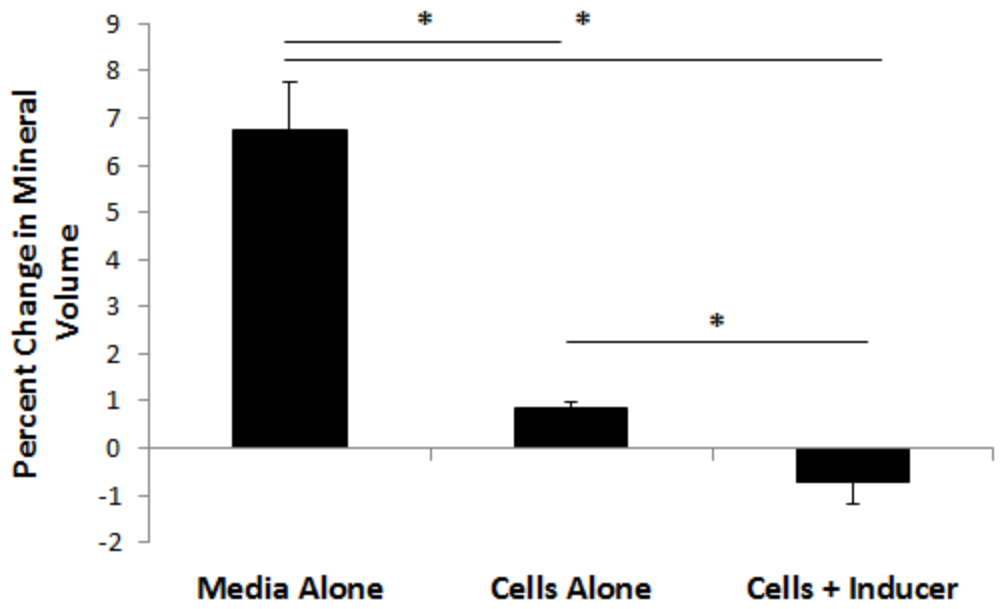

Figure 3.5: Mineral volume decreased in discs seeded with engineered osteoclasts in the presence of inducer. Discs were cultured in media alone or in the presence of inducer for 12 days. In media alone, the discs grew by 6.75%. When seeded with cells the discs only grew by 0.85%, and in the presence of inducer the discs decreased in volume by -0.72%. Data are expressed as mean +/- SD. n = 3-5 discs per condition. *p< 0.05.

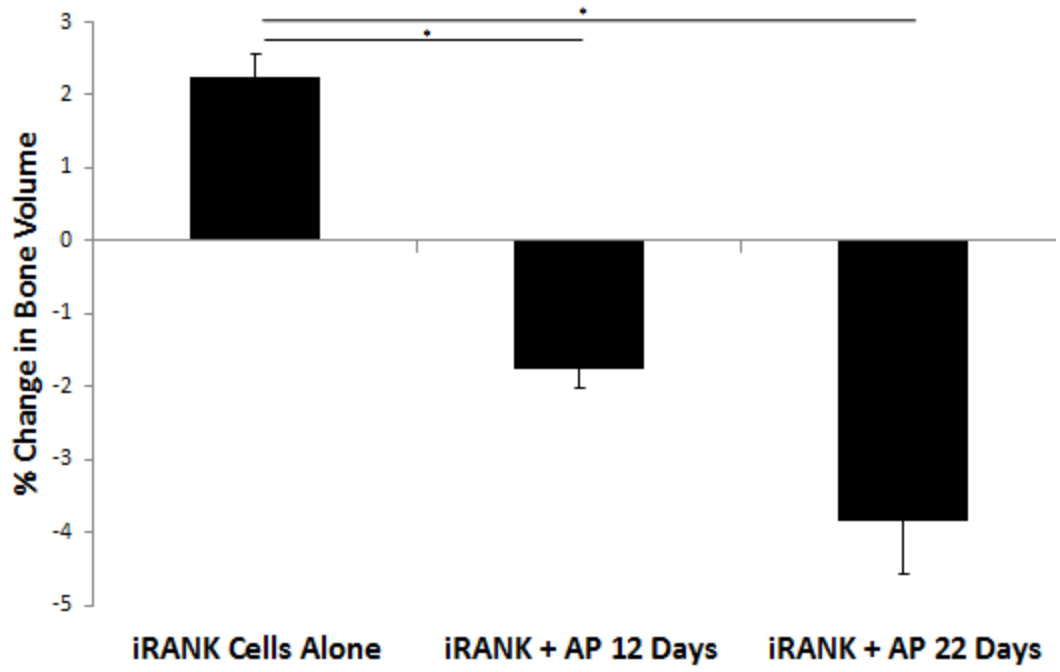

Figure 3.6: Mineral resorption by engineered osteoclasts was enhanced by repeated seeding. Cells were seeded on calvarial discs and cultured in the presence or absence of inducer for 12 days. At this point, discs were cleaned again and re-seeded with cells and cultured for an additional 10 days. With cells alone, the discs grew by 2.24%. Under conditions inducing engineered osteoclast formation, there was significant mineral loss at 12 and 22 days, with mineral loss of -1.77% and 3.84%, respectively. Data are expressed as mean +/- SD. n = 4-6 discs per condition. *$p < 0.05$.

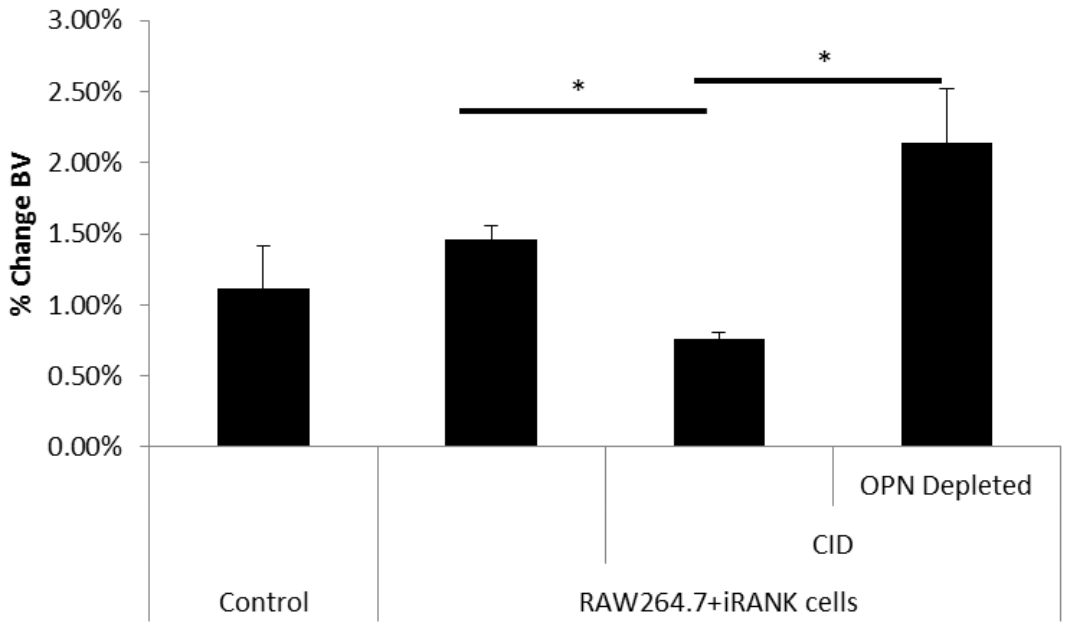

Figure 3.7: Mineral growth in human HO samples was inhibited by conditioned media from RAW264.7+iRANK cells cultured with CID. Samples of human HO were obtained after surgery and sectioned into discs. These were incubated in conditioned media from RAW264.7+iRANK cells cultured in the presence or absence of CID for 5 days. Media from cells cultured with CID inhibited mineral growth. Additionally, when OPN was depleted from the conditioned media, the inhibitory effect was not seen. n = 5 per condition. *$p < 0.05$.

CHAPTER 4

Determining the effects of RAW264.7+iRANK cells on mineral formation and regression in a mouse model of HO

4.1 Abstract

In this chapter, we examined the efficacy of RAW264.7+iRANK cells in preventing mineral formation or resorbing existing mineral *in vivo*. We hypothesized that since the cells were capable of resorbing two and three-dimensional mineral and preventing further mineralization of human HO samples *in vitro*, they would also be effective *in vivo*. First, we developed methods for visualizing the cells *in vivo* in order to ensure that cells remained at the site of injection. We successfully labeled cells with quantum dots and luciferase, but found that bioluminescence allowed us to visualize smaller numbers of cells. Next, we tested cell delivery vehicles, including collagen, fibrin, and BME, for their ability to promote cell retention. We found that collagen allowed for the greatest proliferation while not interfering with osteoclast formation. Finally, we tested our cells *in vivo* in a mouse model of HO. HO lesions were induced by injection of BMP-2 + BME. We tested both RAW264.7+iRANK cells and enriched osteoclasts derived from these cells. The prevention arm received cell injections at Day 14 and 21, while the regression arm received cells at Day 28 and 35. HO lesion volume was measured by microCT before treatment and 1 and 2 weeks later, and tissues were collected after 2 weeks. Finally, we performed histology on explanted tissues and located the HO lesions as well as a mass of GFP-positive cells. Work is ongoing to verify osteoclast formation, but these data provide the first evidence of *in vivo* efficacy of RAW264.7+iRANK cells at treating HO.

4.2 Introduction

Although cell therapy using osteoclasts has been proposed as a treatment for EC and HO, there has been no published work testing this hypothesis *in vivo* [21]. In order to move our proposed cell therapy towards clinical application, *in vivo* efficacy must be demonstrated. Although the *in vitro* data supports the efficacy of our approach, there are many differences between the *in vitro* and *in vivo* environments [57]. We must ensure that the cells are delivered to the desired site, survive and differentiate into osteoclasts, and finally that they have an effect on preventing mineral formation in developing ectopic bone and regressing mineral from existing ectopic bone. To accomplish these goals, we developed methods for visualizing the cells *in vivo* using fluorescence and bioluminescence, retaining cells at the site of injection using cell delivery vehicles, and quantifying *in vivo* effects using a mouse model of HO.

4.2.1 In vivo visualization of cells

Two major methods of visualizing cells *in vivo* are fluorescence and bioluminescence. Fluorescent imaging is based on the ability of certain molecules and particles to absorb light at a specific wavelength and the re-emit the energy at a different one [58]. Quantum dots are small semiconductor particles which can be designed to fluoresce at specific wavelengths. Importantly, murine macrophages have been shown to uptake spontaneously when incubated together [59]. Bioluminescent imaging is different in that it is based on detecting light released by an enzymatic reaction, typically the luciferase enzyme reacting with its substrate luciferin [60]. Both techniques were compared *in vitro* and *in vivo* in mice using a Xenogen *In Vivo* Imaging System (IVIS) to determine which provides the strongest signal.

4.2.2 Cell delivery vehicles

A variety of cell delivery vehicles have been studied for their ability to localize cells, while preserving cell health [61]. Collagen is an ECM protein which is the most abundant protein in animals, while fibrin forms in the final step of the clotting cascade. Basement Membrane Extract (BME) is a mixture of soluble proteins derived from a tumor model. Each of these hydrogels has certain disadvantages. For example, collagen requires a pH neutralization step, which exposes cells to extremes of pH. Fibrin requires thrombin for enzymatic gelation of fibrinogen. Thrombin has been suggested to inhibit osteoclastogenesis *in vitro* which may negatively impact our system [62]. BME is a mixture of several different proteins that could influence osteoclast formation. For these reasons, we will pursue all of the aforementioned delivery vehicles for these studies to determine the optimal delivery vehicle.

4.2.3 Murine HO model

There are a wide variety of animal models of EC and HO using techniques such as genetic modification, protein delivery, biomaterial implantation, and traumatic injury [63]. The model used in the following studies is based on injecting bone morphogenic protein 2 (BMP-2) dissolved in a hydrogel into the calf muscle of mice. This induces the formation of an HO lesion in the muscle over the course of a few weeks which is detectable by microCT allowing for longitudinal quantitation. It has been used by other groups to study HO development [48,64]. We chose to use athymic mice to minimize the possibility of an immune response to the RAW264.7+iRANK cells. Although the cells are derived from mice, it was not possible for these studies to use autologous cells.

4.3 Materials and Methods

4.3.1 Cell culture and generation of osteoclasts

RAW264.7 cells were obtained from ATCC (Manassas, VA) and cultured in D-MEM media from Invitrogen (Carlsbad, CA) containing 10% (v/v) heat-inactivated FBS and 100 U/mL Pen/Strep (Invitrogen) and incubated at 37°C with 5% CO_2. These cells were engineered to contain an inducible RANK receptor (iRANK) as previously described.

4.3.2 Quantum dot loading

Quantum dots (QD) with an emission wavelength of 600 nm (gift of the Gao Lab) were incubated with the cells various concentrations (0-10 nM) for 2 h before replacing the media. Quantum dot loading was verified by fluorescent microscopy and quantified by overlaying the light and fluorescent images and counting cells containing QD.

4.3.3 Lentiviral production and transduction of luciferase gene

The packaging plasmids pSL3 (vesicular stomatitis virus G envelope), pSL4 (HIV-1 gag/pol packing genes) and pSL5 (rev gene required for HIV-1 envelope protein expression) were a gift from the Murry Lab. The transfer plasmid pLEL (luciferase gene) was a gift from the Pub Lab. The lentiviral vector was packaged in HEK293T cells as previously described [65-66] with the following modifications. Briefly, a total of 5×10^6 of HEK293T cells were seeded in 10-cm dishes treated with poly-D-lysine 24 h prior to transfection and the culture media was changed just before transfection. A total 20 µg plasmid DNA (7.5 µg pLEL, 2.5 µg pSL3, 6.7 µg pSL4 and 3.3 µg pSL5) was used for the transfection of one dish. The plasmids were added to 4 mL of Opti-MEM (Thermo Fisher Scientific). This was combined with 4 mL of Opti-MEM to which

120 µL of Lipofectamine 2000 has been added (Thermo Fisher Scientific). The solution was added to the cultures and the media replaced after 14-16 h. The media containing virus was collected after another 48 h and filtered through a 0.45-µm filter. Various volumes of the media containing virus was applied to the target cells, RAW264.7+iRANK for overnight incubation. Transduced RAW264.7+iRANK+Luc cells were allowed to expand before use. Luciferase expression was confirmed and quantified via luminometer.

4.3.4 In vivo visualization of RAW264.7+iRANK cells

Fluorescence and bioluminescence were compared as methods for visualizing the cells *in vivo.* Varying numbers of cells labeled by either method were injected subcutaneously in a mouse, starting at $1x10^5$ and increasing until the cells could be detected with a Xenogen In Vivo Imaging System (IVIS) (Caliper Life Sciences). For the luciferase-labeled cells, the mouse was injected with 150 mg/kg luciferin just prior to imaging.

4.3.5 Developing cell delivery vehicles for in vivo delivery

We tested collagen, fibrin, and Basement Membrane Extract (BME) as cell delivery vehicles. To formulate the collagen carrier, acid-solubilized collagen was diluted with both 10X PBS and a solution of 10 N sodium hydroxide to give final concentration of 0.5 mg/mL collagen. The solution was kept on ice until injection. To formulate the fibrin carrier, fibrinogen dissolved in 0.9% saline was combined with a cell suspension and thrombin immediately before injection for a final concentration of 0.5 mg/mL fibrin. To formulate the BME carrier, frozen Cultrex BME (Trevigen Inc., Gaithersburg, MD, USA) was thawed overnight and diluted with PBS to a final concentration of 0.5 mg/mL BME. For each of these, cells were added immediately before injection.

4.3.6 Serum gradient separation of osteoclasts

To create an enriched osteoclast population, a method for serum gradient purification of osteoclasts was adapted [67]. Briefly, RAW264.7+iRANK cells were seeded on 10-cm plates at $2.5x10^6$ cells per dish and cultured with 50 nM AP20187 for 4 days. Cells were lifted with a cell scraper and placed into a serum gradient above two bottom layers of 40% and 70% FBS. After 25 min, the bottom layer of the serum gradient was collected and placed in a 4-well chamber slide to verify osteoclast enrichment or used for *in vivo* experiments. Osteoclasts were identified by staining for TRAP using a commercial kit according to the manufacturer's instructions.

4.3.7 In vivo model of HO

HO formation was induced in athymic mice using BMP-2. Mice were anesthetized and the mid-belly of the calf muscle was injected with a mixture of recombinant human BMP-2 (Syd Labs Inc., Boston, MA, USA) and Cultrex BME (2.5 µg BMP-2/20 µL of BME). The HO lesions were allowed to form for either 14 or 28 days before cell delivery.

4.3.8 In vivo microcomputed tomography

MicroCT was used to verify HO formation and quantitate the lesion volume. Mice were anesthetized with isoflurane and scanned by microCT (Scanco vivaCT 40; 21-µm voxel resolution 55 kVP, 145 µA). Automated imaged analysis was used to measure bone volume (BV) and tissue volume (TV) with a threshold of 250.

4.3.9 Prevention and regression of HO in vivo

We tested the ability of RAW264.7+iRANK cells to prevent the formation of HO lesions and resorb existing lesions. For the prevention arm, HO lesions were scanned by microCT before receiving $5x10^6$ cells in 25 µL of collagen carrier at day 14. 6 mice received RAW264.7+iRANK cells and 6 received serum gradient enriched osteoclasts. Additionally, 5 control animals received no injections. After the cell injection, CID was administered intraperitoneally daily for three days and then every other day. For injection, CID was formulated with 10% PEG 400 and 1.7% Tween 20, and animals received 2 mg/kg bodyweight at each injection [68]. Animals were scanned again after 1 week and received another cell injection. After 2 weeks, a final microCT scan was performed and the entire calf was explanted and fixed in 10% buffered formalin for histology. Procedures for the regression arm were exactly the same as the prevention arm except the first microCT scan and cell injection did not take place until day 28 (Fig. 4.1).

4.3.10 H&E and TRAP Staining

Tissues were first decalcified in a commercial decalcifying solution (Cal-Ex Decalcifier, Fisher Scientific) for 1 week before tissue processing and sectioning. For Hematoxylin and Eosin staining, slides were deparafinnized and placed in Harris hematoxylin solution for 3 min before rinsing. This was followed by 40 s in ammonium water (0.25% v/v). Finally, slides were dipped in Eosin solution 10 times before dehydrating and coverslipping. For TRAP staining, slides were deparafinnized and rehydrated. A commercial kit was used following the manufacturer's instructions. Slides were mounted with Aqua-Mount and images were obtained using an upright microscope.

4.3.11 Immunofluorescence

A polyclonal antibody for GFP was used for immunofluorescent staining (A-11122, Thermo Fisher Scientific). Slides were deparafinnized and rehydrated with TBS-T (10 mM Tris buffer, 150 mM NaCl, 0.5% Tween-20, pH 7.6) before antigen retrieval was performed. Slides were incubated in boiling citrate buffer (10 mM citrate, 0.05% Tween-20, pH 6) for 5 min and allowed to cool. Blocking was performed with 4% normal donkey serum (NDS) for 1 h before adding the primary antibody. The anti-GFP antibody was diluted in 2% NDS at a ratio of 1:400 and incubated at 4°C overnight. Slides were rinsed 3X in TBS-T for 5 min each before adding the secondary antibody. Cy3 AffiniPure Donkey Anti-Rabbit IgG (Jackson ImmunoResearch Laboratories, Inc.) was diluted in 2% NDS at a concentration of 10 µg/mL for 30 min. Slides were rinsed 3X in TBS-T for 5 min each before mounting with ProLong Gold Antifade Mountant (Invitrogen, Carlsbad, CA).

4.3.12 Statistical analysis

For the prevention and regression data, a repeated measures ANOVA with Bonferroni's post-hoc test was used to compared each time point within a given treatment group to determine if there was a significant change from baseline. A p-value of less than 0.05 was considered significant.

4.4 Results

4.4.1 Cell labeling with quantum dots

Macrophages were found to readily phagocytize QDs in culture. When incubated with QDs, the highest loading was found at 10 nM QD with 90% of cells labeled (Fig. 4.2A). We also examined the effect of QD-loading on OC formation to ensure that they were not inhibiting OC

formation by our system (Fig. 4.2B). There was no significant difference between the 8 nM and 10 nM cocentrations, so we did not explore higher concentrations and used 10 nM for subsquent studies.

4.4.2 Transduction of RAW264.7+iRANK cells with a luciferase construct

A lentiviral vector carrying the luciferase gene was produced and used to introduce the luciferase gene into our cell line. Cells were incubated with various volumes of virus supernatent and luminesence from these cell lines was quantified via luminometer (Fig. 4.3A). There did not appear to be a great difference between the 1 mL and 2 mL cell lines, so we proceeded with the 2 mL cell line. We tested the ability of this cell line to form osteoclasts *in vitro* and did not find a difference in the number of TRAP-positive cells we observed (Fig. 4.3B).

4.4.3 In vivo comparison and fluoresence and bioluminesence

We injected varying numbers of the labeled-cells subcutaneously in a mouse and imaged with the Xenogen IVIS. With the QD-labeled cells, signal was first apparent at $5x10^6$ cells, with a stronger signal from $1x10^7$ cells (Fig. 4.4A). Using luciferase, we were able to visualize a smaller numbers of cells *in vivo*, as low as $2x10^5$ cells (Fig. 4.4B). This is likely due to the issue of auto-fluorescence, which results in a lower signal/noise ratio. Additionally, the QDs become diluted over time as cells divide, further diminishing the signal. For these reasons, we used the luciferase-labeled cells for future experiments

4.4.4 In vivo testing of cell delivery vehicles

From the pilot *in vivo* experiment, we were able to determine that all delivery vehicles (no gel, collagen, fibrin, BME) were able to deliver and retain cells in the calf (Fig. 4.5). Qualitatively,

both PBS (Fig. 4.5A) and collagen (Fig. 4.5B) had good cell delivery to both limbs. Fibrin (Fig. 4.5C) had very uneven delivery, most likely due to the fact that it was difficult to inject the delivery vehicle because the fibrin clotted within the syringe. BME (Fig. 4.5D) was the least viscous of three gels and the cells were not retained at the site of injection.

The bioluminescence data was quantified and the signal increased over time in all conditions. This suggests that the cells proliferated, which was expected as the engineered osteoclasts were derived from a cell line and were injected into athymic mice (Fig. 4.6). Fibrin has the lowest signal followed by BME. Collagen was higher than the PBS control at every time point, so it was used for the next set of experiments. The data presented here ends at Day 8 but signal could still be detected at Day 15. This data was excluded because the detector was saturated in the collagen gel condition.

4.4.5 Osteoclast enrichment

RAW264.7+iRANK cells were pre-treated with CID before placing into a serum gradient column. After 25 minutes of separation, the layers were collected and the cells cultured briefly before performing fixation and TRAP staining. The top layer of the gradient (Fig. 4.7A) mainly consisted of small mononuclear TRAP-negative cells while the bottom layer (Fig. 4.7B) was enriched with large multinucleated TRAP-positive cells, indicating successful purification of osteoclasts.

4.4.6 HO lesions formed in vivo

We injected mice with BMP-2 and BME to induce the formation of HO lesions before measuring the lesion volume by microCT (Fig. 4.8).

4.4.7 Prevention of HO formation

We injected RAW264.7+iRANK cells or enriched osteoclasts at sites of HO at Days 14 and 21 after induction of HO formation to examine the effect of the cells on the progression of newly forming HO. We scanned the HO lesions by microCT at Days 14, 21, and 28. Every group decreased over the two-week period, including controls. Three out of five mice in the control group had minimal HO formation, and there were no significant changes in BV (Fig. 4.9A). In the group treated with enriched osteoclasts, there was a significant decrease in TV at Days 21 and 28 compared to Day 14 (Fig. 4.9B).

4.4.8 Regression of existing HO

We injected RAW264.7+iRANK cells or enriched osteoclasts at sites of HO at Days 28 and 35 after induction of HO formation to examine the effect of the cells on stable HO lesions. These mice were scanned by microCT at Days 14, 21, and 28. The control group and the group treated with enriched osteoclasts had relatively stable HO lesions when looking at both BV (Fig. 4.10A) and TV (Fig. 4.10B). However, HO lesions in the RAW264.7+iRANK-treated mice decreased significantly in both BV and TV compared to baseline.

4.4.9 HO lesions were found in histology

We successfully decalcified the calves of mice. Through H&E staining, we were able to identify the tibia (Fig. 4.11A) and the fibula (Fig. 4.11B). We also found a porous structure with a bone-like exterior (Fig. 4.11C). This matches the microCT images of the HO lesions. Near the HO lesions, we found a mass of morphologically distinct mononuclear cells that did not appear to be bone or muscle (Fig. 4.11D).

4.4.10 TRAP staining

We performed TRAP staining on a variety samples from both treated and untreated mice, but we unable to locate TRAP-positive cells. They could not be found in the HO lesion (Fig. 4.12A) or the native bone (Fig. 4.12B), suggesting the decalcification method inactivated the TRAP enzyme, but it is possible we have just missed them in histology. Work is ongoing using an alternative decalcification protocol to determine if TRAP-positive cells can be located in our samples.

4.4.11 GFP-positive cells were co-localized with cells in treated animals

We examined the mass of morphologically distinct mononuclear cells and found GFP-positive cells at the edges (Fig. 4.13A). Importantly, adjacent muscle tissue did not stain positive, suggesting these are the injected cells (Fig. 4.13B).

4.5 Discussion

These studies represent the first *in vivo* work using engineered osteoclasts as a cell therapy for HO. We were able to visualize the cells *in vivo* and verify that they remain at the injection site through the use of a hydrogel delivery vehicle for up to 15 days. HO lesions were induced in athymic mice and cells were delivered to these sites. We used longitudinal microCT scans to determine the effect of the cell on the formation and regression of HO lesions. In the prevention arm, there was a significant decrease in TV compared to baseline in the group treated with enriched osteoclasts. In the regression arm, we found that the group treated with RAW264.7+iRANK cells had significant differences in both BV and TV between every time point. From the histology, we were able to locate the native bone and the HO lesions, as well as a

mass of cells near the HO lesion. TRAP-positive cells were not seen in the HO lesion or native bone, but GFP-positive cells were co-localized with the mass of cells. These results suggest our cells are present and have an effect on the size of the HO lesion, but further study is needed to demonstrate osteoclast formation.

Before testing the cells *in vivo* we wanted to verify that cells survived and stayed at the injection site after delivery. First, we labeled cells for *in vivo* visualization using both fluorescent QDs and bioluminescence by transducing the cells with the luciferase gene. Importantly, we found that neither method affected OC formation *in vitro.* While both methods allowed for the cells to be detected *in vitro* and *in vivo*, the signal was much stronger from bioluminescence. In fact, we found there was almost an order of magnitude difference in the techniques. This is partly due to the fact that there is a great deal of photon attenuation in living tissue. With fluorescent imaging, a photon must travel into the tissue to reach the fluorescent label before being release and traveling out of the tissue for detection. Additionally, mouse skin is known to be auto-fluorescent [69]. For these reasons, bioluminescence was used for the next set of experiments.

To promote cell retention after delivery, we tested various hydrogels as cell delivery vehicles. Cell delivery vehicles are widely using in the field of cell therapy and regenerative medicine [70]. The hydrogels we compared were collagen, fibrin and BME. Cells were suspended in each and injected into the calf muscle of athymic mice and bioluminescence was measured over 2 weeks. Fibrin gels had very uneven delivery due to the gelation process beginning in the syringe and BME had low cell proliferation and retention. Collagen proved easiest to work with and had the highest level of bioluminescence at each time point.

The HO model we used has previously been used to study inhibition of HO formation by botulinum toxin [48]. BMP-2 and BME were injected into the right calf muscle and lesions were allowed to develop over the course of a few weeks. This model has the advantage of being faster than other animal models of HO, but has the disadvantage of being less physiologically relevant than other models, such as trauma based methods [63].

We decided to test both RAW264.7+iRANK cells and osteoclasts which had been formed from this cell line and then purified to enrich them. This was done for a variety of reasons. First, we wanted to guarantee that some osteoclasts were reaching the site of HO. Additionally, we have observed *in vitro* that a certain portion of our cells never undergo osteoclastogenesis but continue to proliferate. This occurs even though we sorted twice by fluorescence-activated cell sorting to >98% purity. A final motivation for testing the enriched cells was that we performed an *in vivo* pilot experiment and the injected limb was seen to grow over the course of 4 weeks. RAW264.7 cells are a cell line and were derived from a virus-induced tumor, so it is not surprising that they continued to proliferate *in vivo* [71]. Using osteoclasts derived from primary cells would be preferable and more physiologically relevant, and extensive effort was expended to develop these. However, using bone marrow derived monocytes yielded so few final osteoclasts that we would need dozens of mice to develop osteoclasts for one mouse being treated. We also investigated developing osteoclasts from human induced pluripotent stem cells, which has been reported in the literature [72]. Our efforts were unable to replicate their methods, but this is an important research goal for translating our therapy to the clinic.

When we tested the cells *in vivo* we found significant changes over time in the groups treated. In the prevention arm, BV and TV trended downward in all groups over the two-week period. This was unexpected for the control group because previous work with this model has shown an

increase in HO lesion volume over the first few weeks. Additionally, three out of five mice in the control group developed almost no HO lesions, despite being injected with the same mixture to induce HO formation. These were the first mice injected and they were all injected with the same syringe, so it is possible that the mixture was not fully mixed yet. The other two control mice did form HO lesions, but these decreased in volume compared to baseline. In the enriched osteoclast-treated group, TV decreased significantly by Day 28 compared to baseline and the change in BV was nearly significant ($p=0.064$). This suggests that the enriched osteoclasts might be influencing the consolidation of the HO lesion, but further study is needed.

In the regression arm, HO formation in the control and enriched-osteoclast remained relatively stable over the two-week treatment period. The trends in the control group mirror previous work with this model [46]. In the RAW264.7+iRANK-treated group, there was a significant decrease in both BV and TV. BV decreased by more than 11% and TV decreased by almost 24%. Every measurement was significantly different from the other two time points, meaning this decrease was detectable after only 1 week of treatment, but also that the effect continued during the second week of treatment.

Histology allowed us to more closely examine the local environment. We located the HO lesions, as well as the tibia and fibula. The HO lesions were porous inside and mineralized on the exterior. This is the same kind of structure seen in the microCT scans, suggesting that our identification is positive and our decalcification and histological methods are producing representative images of the tissue. We also noticed a mass of morphologically distinct mononuclear cells near the HO lesion in the treated animals, but not in the untreated animals. Unfortunately, we have not been able to locate any TRAP-positive cells with the tissue, including the native bone. This fact combined with the fact that multiple sets of reagents were

tested, suggests that the decalcification method may have inactivated the TRAP enzyme. The decalcifying solution used contains both ethylenediaminetetraacetic acid (EDTA) and hydrochloric and the acid may have affected TRAP activity. We are currently decalcifying tissues in an EDTA solution, and are also testing another method of labeling the tissue called OsteoSense, which is a fluorescent stain for bisphosphonates. Despite the lack of TRAP-positive cells in our sections, we were able to find GFP-positive cells. They appeared on the periphery of the mass of mononuclear cells and could be co-localized with these cells but not with the surrounding muscle. This result suggests that our injected cells are remaining near the HO lesion, but it is still not clear how they are affecting HO volume.

4.6 Limitations

In this chapter we developed methods for delivering and visualizing RAW264.7+iRANK cells *in vivo* and measured their effect on a murine model of HO. The biggest limitation of this study as mentioned before was the use of a cell line, rather than primary cells. These cells proliferated extensively *in vivo* and limited the length of our experiments. The use of this cell line contributed directly to the second limitation of these studies, which was the use of athymic mice. These mice were used to minimize immune rejection of the cell line, but these mice have an immune response which differs greatly from wild-type mice. Another significant limitation was the mouse model we used, which involved injecting exogenous BMP-2 into the calf muscle of the mice. This model has been used by other groups, but it is very different from the development of HO, which occurs after injury. An injury-based mouse model could provide a more physiologically relevant system to test our cell therapy.

4.7 Conclusions

In this chapter, the ability of RAW264.7+iRANK cells was investigated. First, cells were labeled using fluorescent QDs and bioluminescence. Bioluminescent labeling using the luciferase gene provided a much stronger signal. Cell delivery vehicles, including collagen, fibrin, and BME, were developed and compared *in vivo*. Collagen had much better handling properties than fibrin and BME and had a higher bioluminescent signal than control. HO lesions were formed in the calf muscle of athymic mice and scanned by microCT. RAW264.7+iRANK cells and enriched osteoclasts derived from this cell line were delivered to these lesions in collagen. We found that RAW264.7+iRANK cells significantly reduced HO lesion size as measured by BV and TV compared to baseline. Additionally, we located a mass of GFP-positive cells near the HO lesion. Work is ongoing with TRAP staining to help us determine exactly how the RAW264.7+iRANK cells are acting upon the HO lesion.

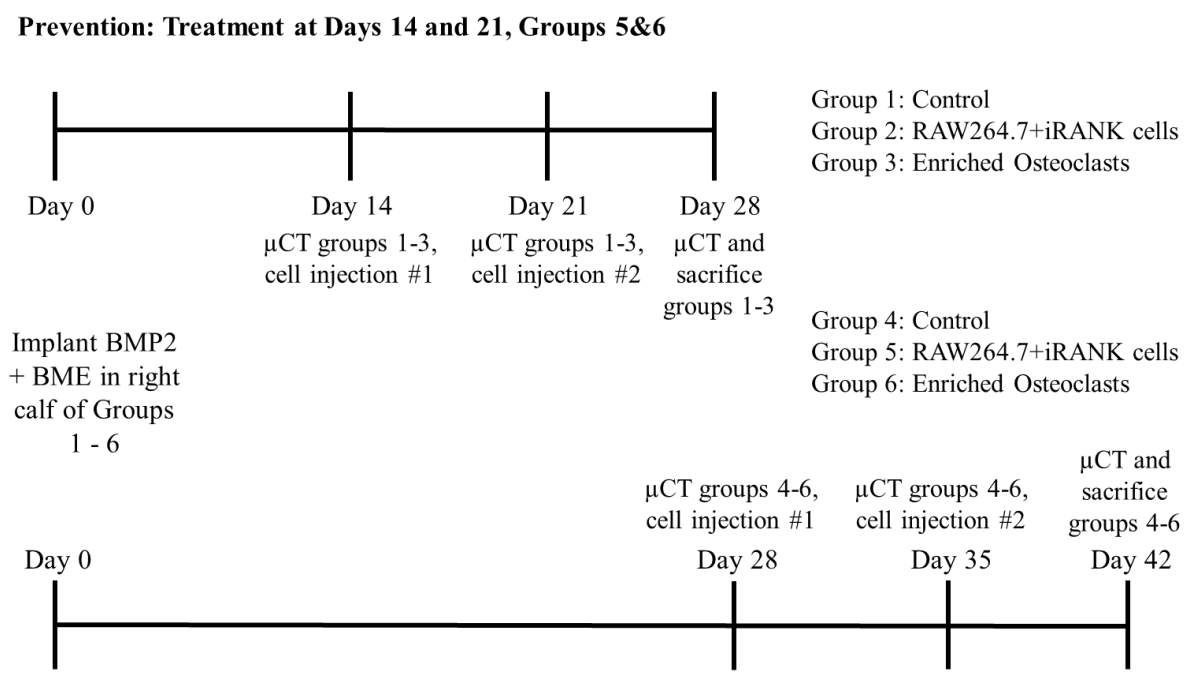

Figure 4.1: Experimental timeline. HO lesions were induced at Day 0 by injecting a mixture of BMP-2 and BME into the right calf muscle. Prevention and regression of mineral was examined. In the prevention arm, mice were scanned by microCT after 14 days to measure the volume of the HO lesion. They then received an injection of RAW264.7+iRANK cells or enriched osteoclasts derived from this cell line. Control mice received no cells and CID was injected intraperitoneally to stimulate osteoclastogenesis. Mice were scanned again one week later at day 21 and received a second injection of cells and additional injections of CID. At Day 28, a final scan was performed and the mice were sacrificed and tissues collected for histology. In the regression arm, procedures were similar except the scans and cell injections took place at Day 28 and 35. Mice in these groups were sacrificed at Day 42 and tissues collected.

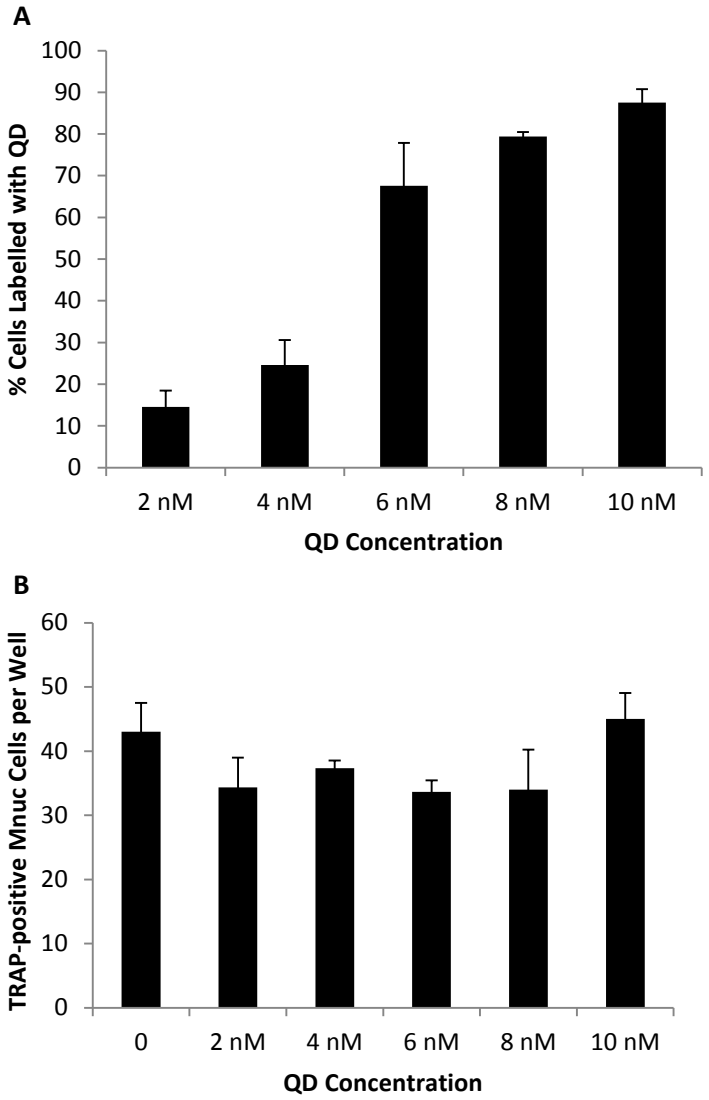

Figure 4.2: QD Labeling of RAW264.7+iRANK Cells. (A) QDs were readily taken up by our cell line with the highest labeling of 90% occurring at the 10 nM concentration. (B) QDs did not significantly affect osteoclast formation as measured by the number of TRAP-positive multinucleated cells seen in culture, even at the highest concentration. n = 3 wells per condition.

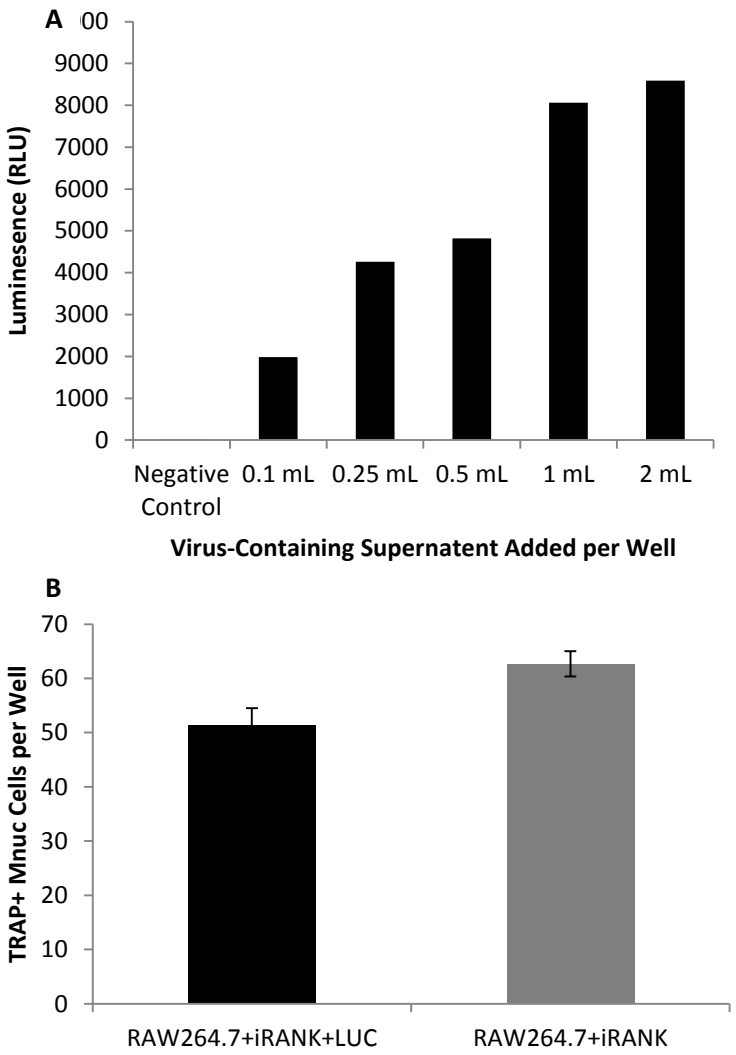

Figure 4.3: Transduction of the Luciferase Gene into RAW264.7+iRANK Cells. (A) Luminescence increased in a dose-dependent manner with increasing volumes of virus-containing supernatant. (B) Cells which were transduced with the luciferase gene had slightly fewer TRAP-positive multinucleated cells but this was not significant. n = 3 wells per condition for the osteoclast assay.

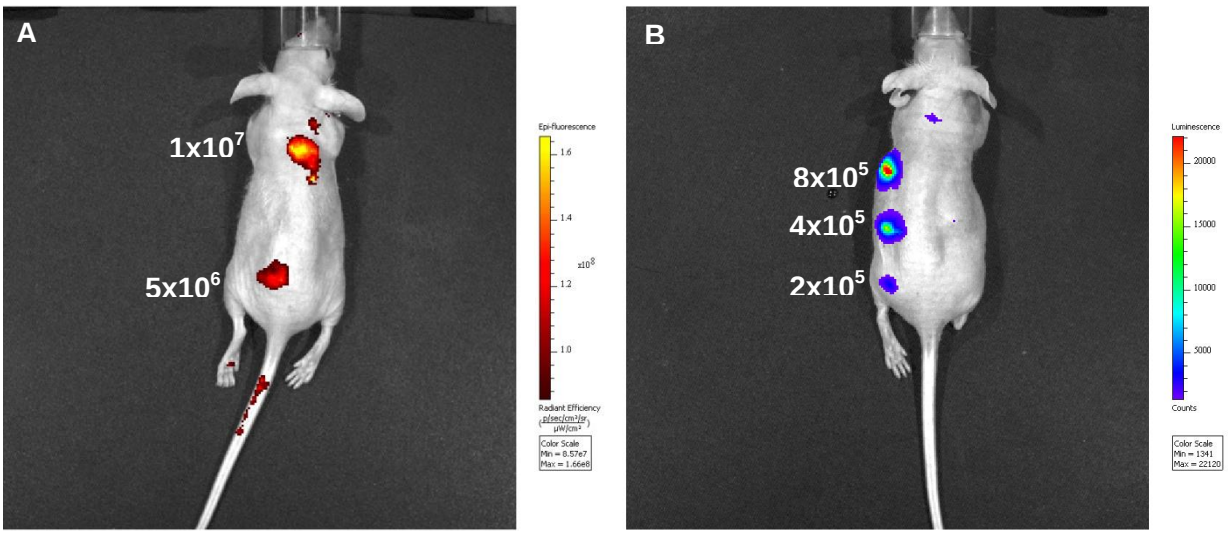

Figure 4.4: Comparison of fluorescence and bioluminescence for *in vivo* imaging. (A) RAW264.7+iRANK cells were labelled with QDs and injected into mice. The minimum number of cells to detect a signal was $5x10^6$ cells. (B) Luciferase expressing RAW264.7+iRANK cells could be detected with as few as $2x10^5$ cells.

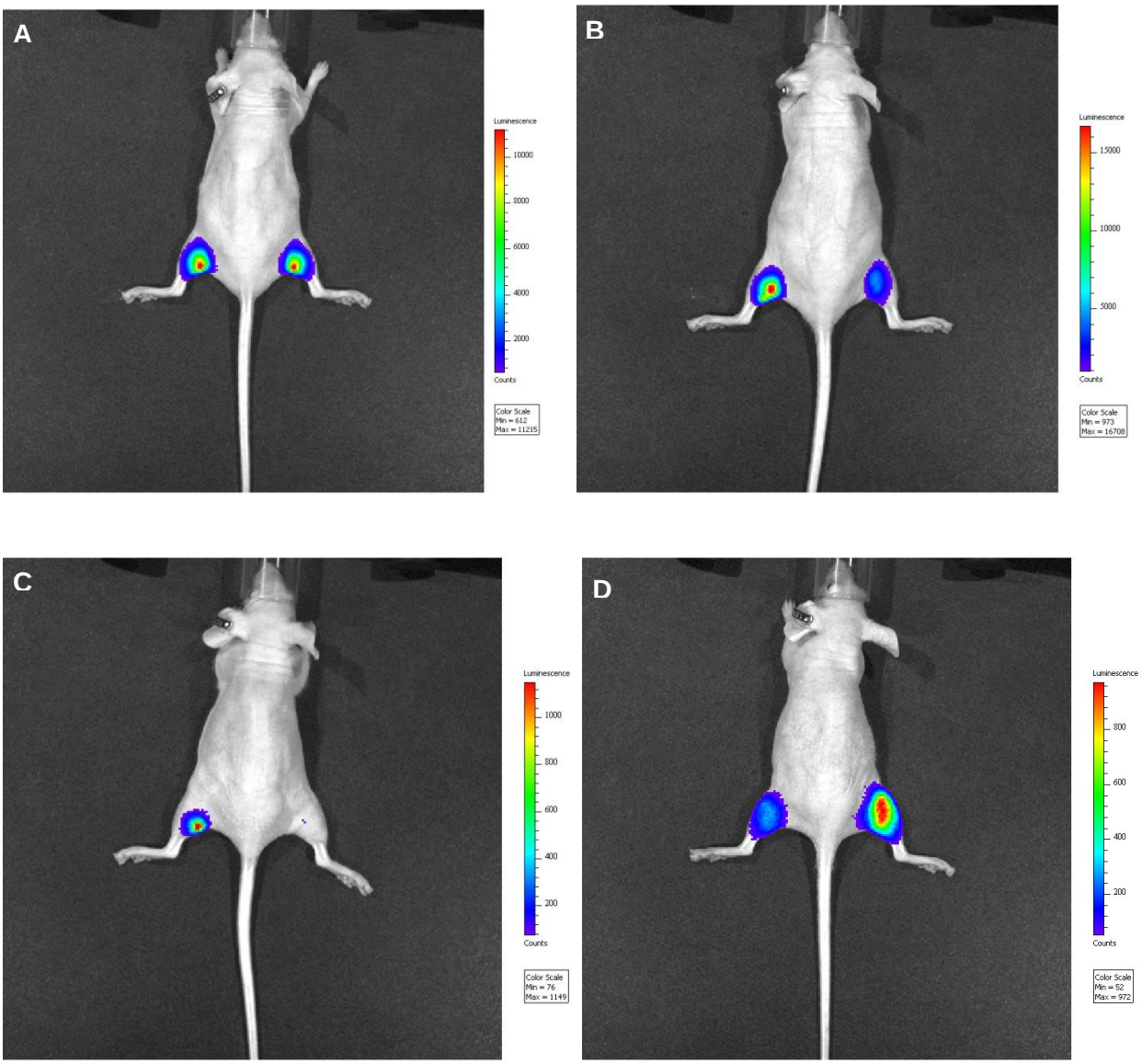

Figure 4.5: Engineered cells could be visualized by bioluminescence in every delivery vehicle. B&W image bioluminescent signal overlay at Day 8. (A) PBS control, (B) Collagen, (C) Fibrin, (D) BME.

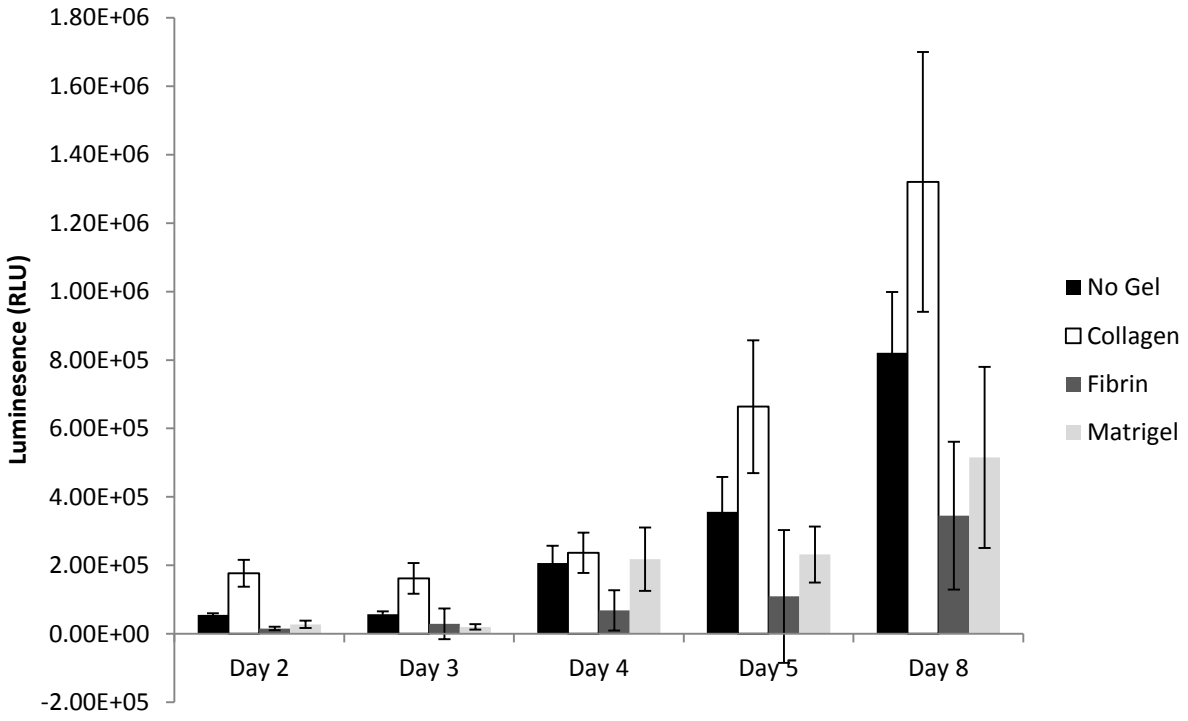

Figure 4.6: Bioluminescent signal increased over time in all conditions. Collagen had the highest signal at every time point, followed by the no gel condition. Each condition had two mice, which received bilateral injections for a total of 4 injection sites per condition.

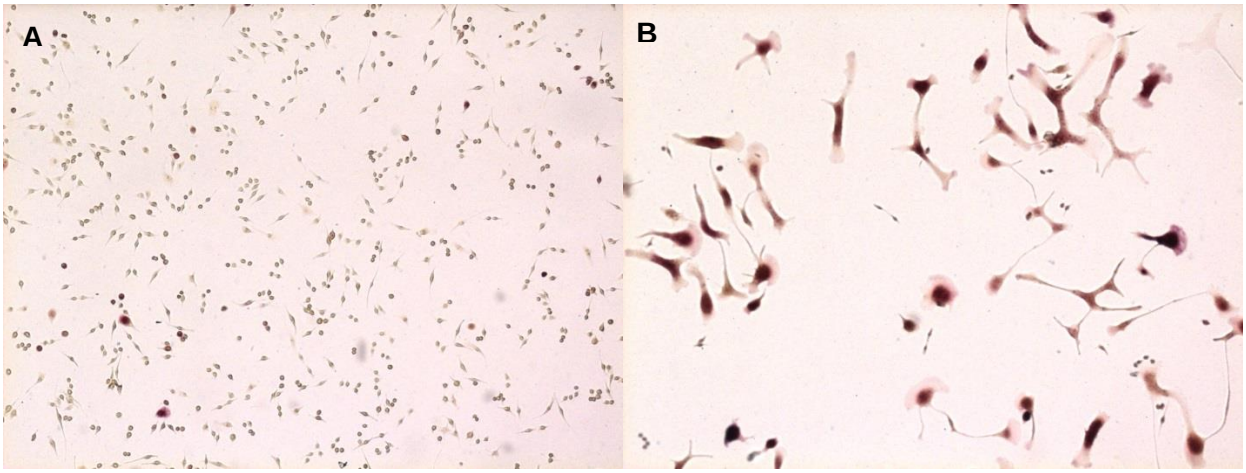

Figure 4.7: Serum gradient purification of osteoclasts. (A) Top layer of serum gradient with mononuclear TRAP-negative cells (B) Bottom layer of serum gradient enriched in TRAP-positive multinucleated osteoclasts.

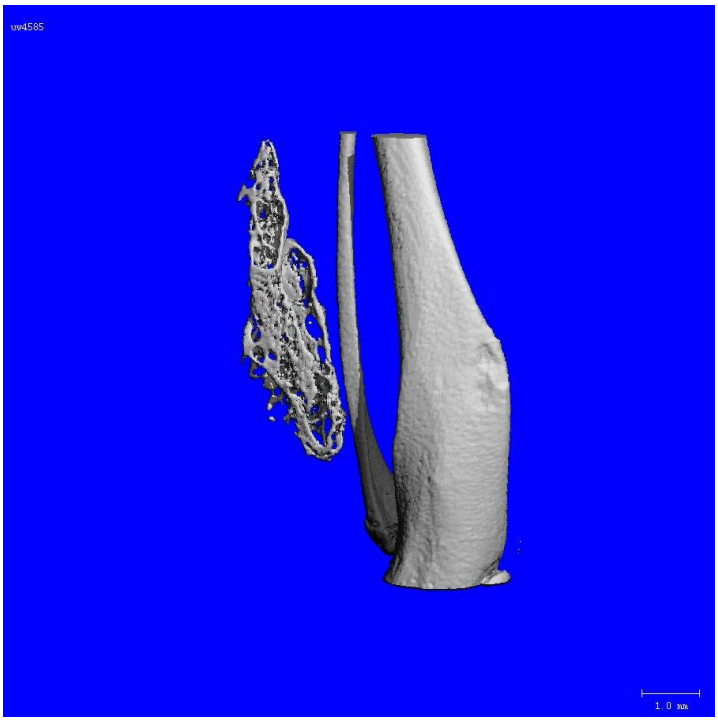

Figure 4.8: HO lesion with tibia and fibula at Day 28. HO lesions were induced by injecting BMP-2 and BME into the calf muscle of athymic mice.

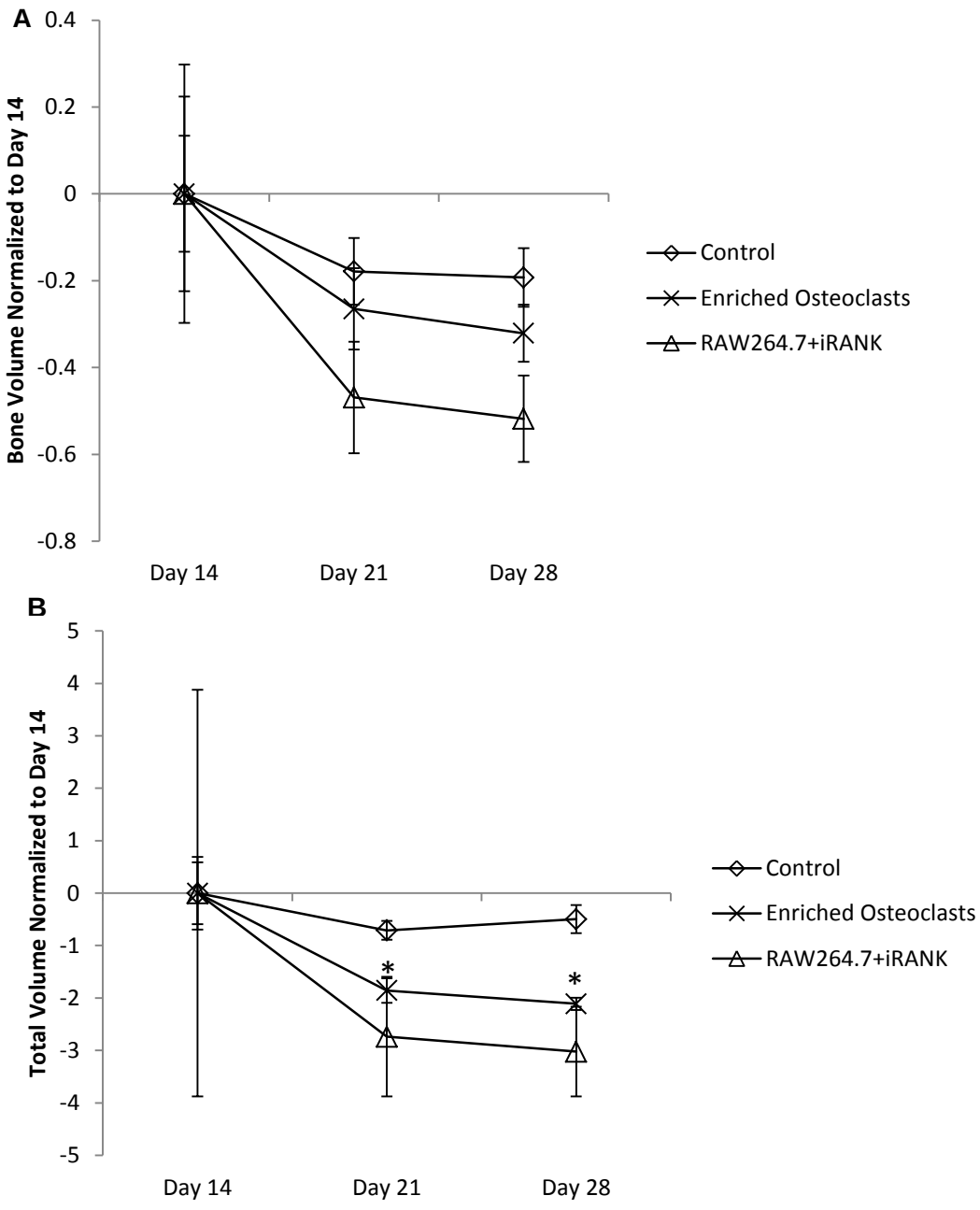

Figure 4.9: Change in BV and TV normalized to Day 14. (A) The group treated with RAW264.7+iRANK cells had the largest decrease in BV but this was not significant. (B) The group treated with enriched osteoclasts had a significant decrease in TV. n = 5-6 animals per condition. *$p<0.05$ comparing that time point to Day 14 by repeated measures ANOVA.

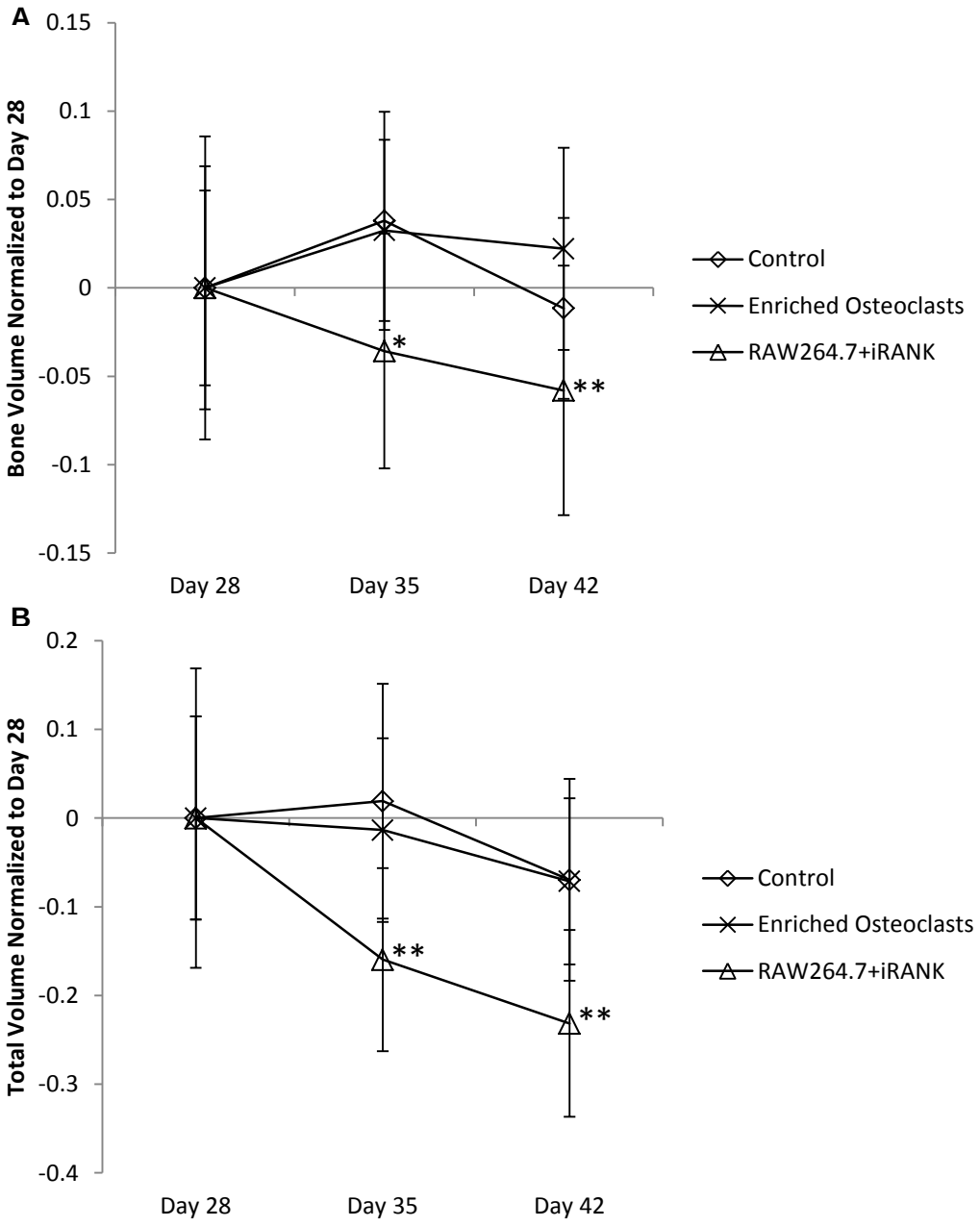

Figure 4.10: Change in BV and TV normalized to Day 28. The group treated with RAW264.7+iRANK cells had a significant different between every time point in both BV (A) and TV (B). n = 5-6 animals per condition. *$p<0.05$ and **$p<0.01$ comparing that time point to Day 28 by repeated measures ANOVA.

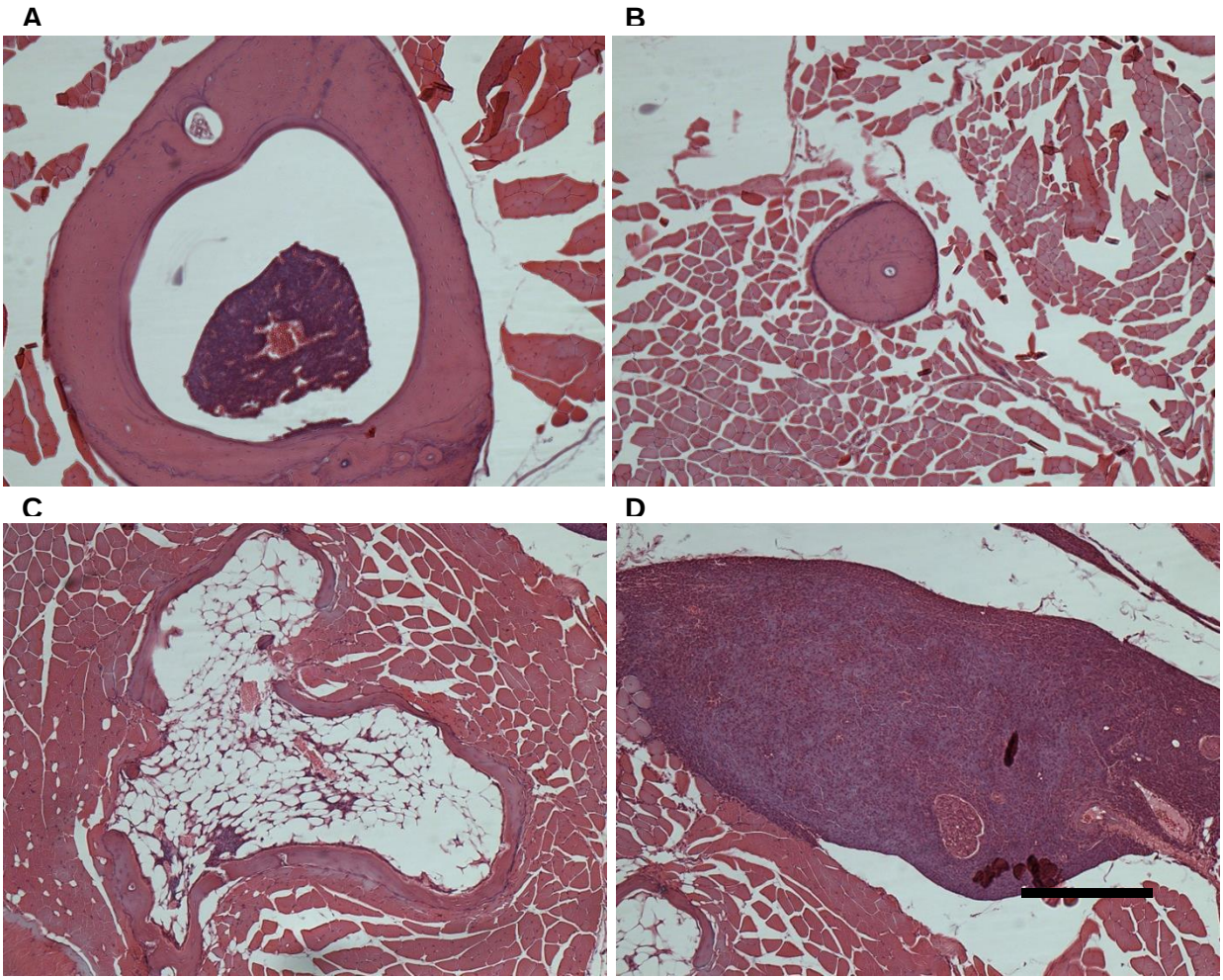

Figure 4.11: H&E staining of calf from treated mouse. (A) Tibia and (B) fibula could be identified. (C) The HO lesion appeared as a porous structure with a more mineralized surface as seen in microCT scans. (D) A large mass of cells could be seen in the treated mice, but not the untreated mice. The HO lesion can be seen in the lower left corner. Scale bar = 50 µm.

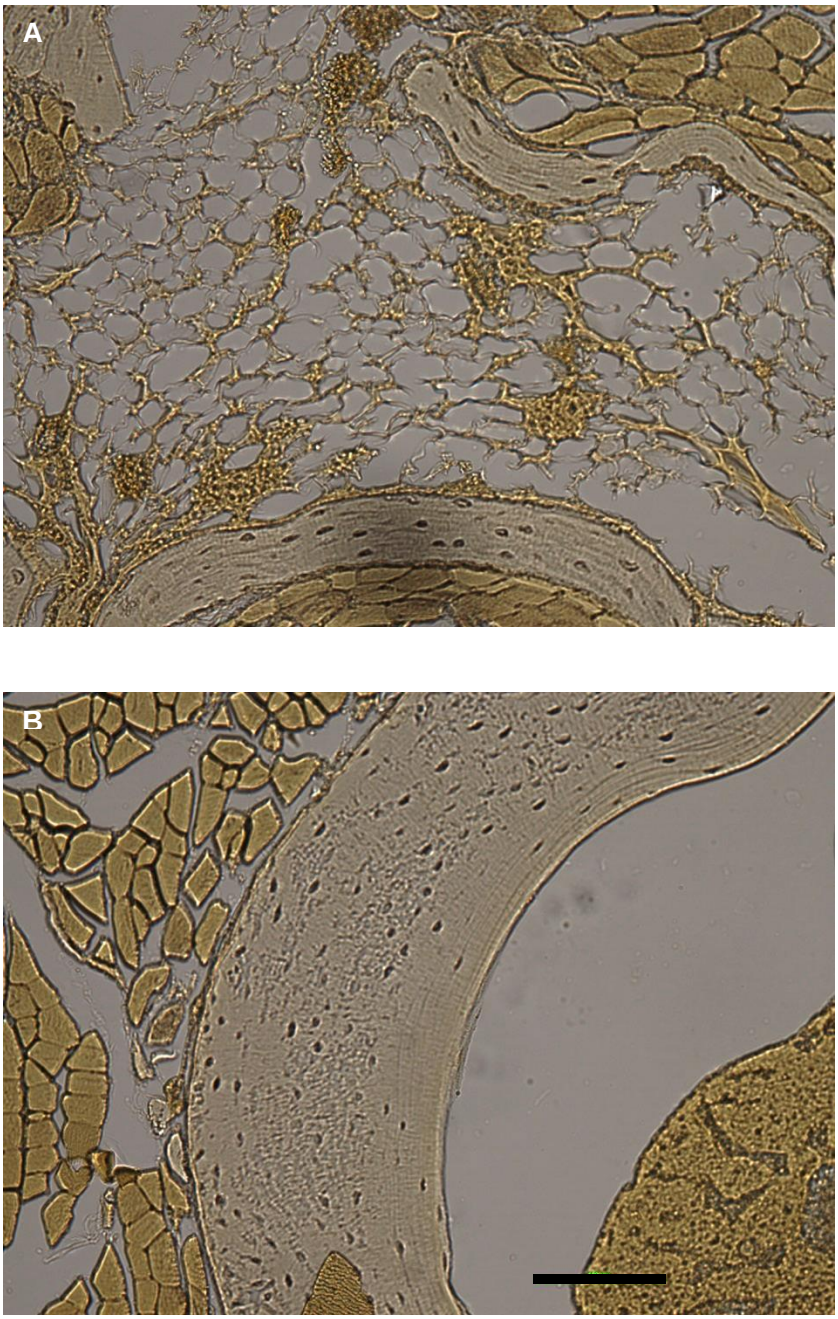

Figure 4.12: TRAP staining of HO lesion and tibia. TRAP-positive cells have not been located within the HO lesion (A). They were also have not yet been found within native bone (B). Scale bar = 100 μm.

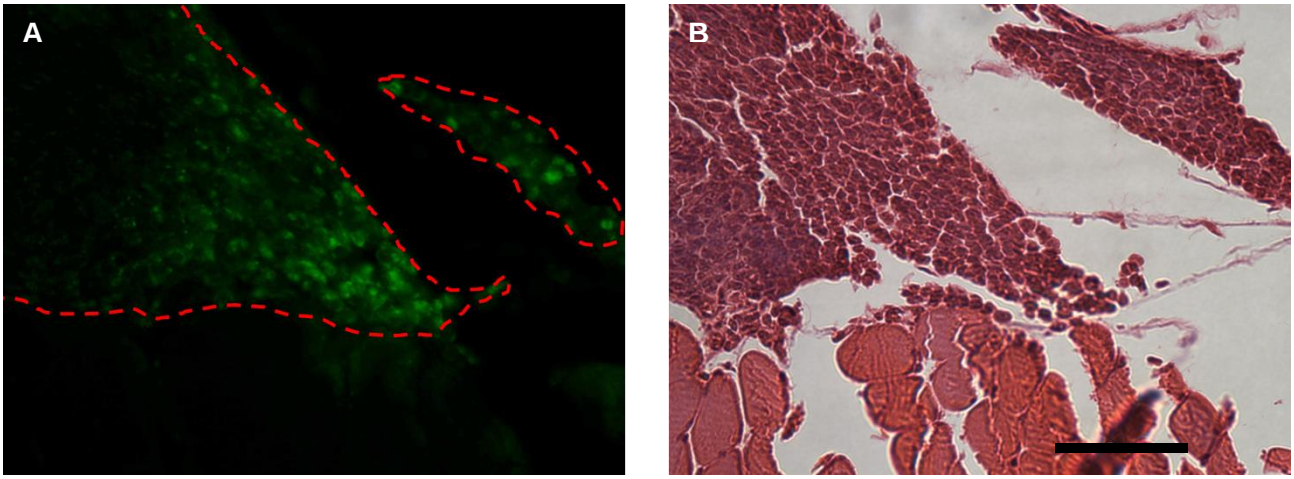

Figure 4.13: GFP and H&E staining of adjacent slides. GFP-positive cells (A) could be detected at the boundary of the mass of cells (B). Scale bar = 50 µm.

CHAPTER 5

Overall conclusions

The CID system has been previously used for a variety of applications, but had never been successfully applied to osteoclast differentiation. One previous attempt that failed relied on only one CID-binding domain, but we demonstrated that two binding domains allows for the trimerization necessary for osteoclastogenesis. This finding is useful to applying the CID system to other receptors, many of which undergo trimerization like RANK. We tested our iRANK construct in a mouse macrophage cell line and verified that these cells could form osteoclasts using both biochemical and functional assays. We then developed three-dimensional *in vitro* models to test the resorptive abilities of the RAW264.7+iRANK cells and found they could both resorb existing mineral and prevent further progression of mineral formation. These models may prove useful to quantifying osteoclastic resorption in other situations. Finally, we tested our therapy in a mouse HO model and found that the cells could significantly reduce volume of the HO lesions compared to baseline. We also located the cells we delivered in close proximity to the HO lesions. Studies of resorption rate in osteoclasts have reported that each osteoclast can resorb ~400 μm^3/h [73]. If our engineered osteoclasts survive for 10 days *in vivo,* a little over $1x10^4$ osteoclasts would be needed to resorb each cubic millimeter of mineralized tissue, suggesting this therapy could be scaled.

Work is ongoing to determine if the cells are forming osteoclasts that resorb mineral *in vivo* or if CID stimulation is causing the RAW264.7+iRANK cells to secrete factors that act upon either the HO itself or endogenous cells to cause mineral resorption or limit its progression. TRAP staining will allow us to better answer this question. The two and three-dimensional resorption

data combined with the ability of conditioned media to inhibit mineralization of human HO samples suggest that RAW264.7+iRANK cells have a variety of mechanisms for affecting both cells and mineral. Taken together, this work provides the first *in vitro* and *in vivo* evidence that a cell therapy using engineered osteoclasts could be used to treat EC and HO.

CHAPTER 6

Future studies

Work using cells containing the engineered construct is proceeding on several fronts but there are a variety of studies that would help this research progress towards the clinic.

6.1 Testing the iRANK construct in primary cells

One major limitation of the studies described here are that we used a cell line. In addition to be less physiologically relevant than primary cells, using a cell line presented us with difficulties along the way when cells proliferated excessively *in vitro* and *in vivo.* As mentioned earlier, we tried both primary cells from bone marrow and human iPSCs unsuccessfully. As part of another study, we are developing a transgenic mouse containing the iRANK construct in cells of the myeloid lineage. These mice could be an excellent cell source for future experiments as it would eliminate the low yield seen when transducing primary cells with the iRANK construct. It would also limit the cell overgrowth we saw in some of the *in vivo* pilot experiments, which limited the length of the experiments and the number of cell injections.

6.2 Contact Independent Inhibition of Mineral Formation

Our lab is currently exploring the mechanisms by which RAW264.7+iRANK cells can inhibit mineral formation. As mentioned in Chapter 3, conditioned media from RAW264.7+iRANK cells cultured with CID inhibits passive mineral growth in human HO samples, but this effect is not seen without CID. Additionally, depletion of OPN also negates the effect. Interestingly, we have also observed the same effect in calcification assays using both bovine valve interstitial cells and C2C12 myoblasts. OPN depletion in these assays reduces the effect suggesting it plays

a major role, but there are many other candidate proteins that may be involved. In order to understand the various effects that our system is capable of proteomic studies are needed.

REFERENCES

1. Giachelli CM (1999) Ectopic calcification: gathering hard facts about soft tissue mineralization. Am J Pathol 154: 671-675.

2. Stewart BF, Siscovick D, Lind BK, Gardin JM, Gottdiener JS, Smith VE, Kitzman DW, Otto CM (1997) Clinical factors associated with calcific aortic valve disease. Cardiovascular Health Study. J Am Coll Cardiol 29(3):630-4.

3. Sverdlov AL, Ngo DT, Chapman MJ, Ali OA, Chirkov YY, Horowitz JD (2001) Pathogenesis of aortic stenosis: not just a matter of wear and tear. Am J Cardiovasc Dis 1(2):185-99.

4. O'Brien KD (2007) Epidemiology and genetics of calcific aortic valve disease. J Investig Med 55:284-291

5. Chang YT, Wu JL, Hsu CC, Wang JD, Sung JM (2014) Diabetes and end-stage renal disease synergistically contribute to increased incidence of cardiovascular events: a nationwide follow-up study during 1998-2009. Diabetes Care 37(1):277-85.

6. McCarthy EF, Sundaram M (2005) Heterotopic ossification: a review. Skeletal Radiol 34(10):609-19.

7. Davies OG, Grover LM, Lewis MP, Liu Y. PDGF is a potent initiator of bone formation in a tissue engineered model of pathological ossification. J Tissue Eng Regen Med. 2016 Oct 3.

8. Melcer T, Belnap B, Walker GJ, Konoske P, Galarneau M. Heterotopic ossification in combat amputees from Afghanistan and Iraq wars: five case histories and results from a small series of patients. J Rehabil Res Dev. 2011, 1-12.

9. Siddiqui RF, Abraham JR, Butany J (2009) Bioprosthetic heart valves: modes of failure. Histopathology 55(2):

10. Wu M, Rementer C, Giachelli CM (2013) Vascular calcification: an update on mechanisms and challenges in treatment. Calcif Tissue Int 93(4):365-73.

11. Polfer EM, Forsberg JA, Fleming ME, Potter BK (2013) Neurovascular entrapment due to combat-related heterotopic ossification in the lower extremity. J Bone Joint Surg Am 95(24):e195(1-6).

12. Pellegrini VD Jr, Gregoritch SJ (1996) Preoperative irradiation for prevention of heterotopic ossification following total hip arthroplasty. J Bone Joint Surg Am 78(6):870-81.

13. Iwamoto K, Miyamoto T, Sawatani Y, Hosogane N, Hamaguchi I, et al. (2004) Dimer formation of receptor activator of nuclear factor kappaB induces incomplete osteoclast formation. Biochem Biophys Res Commun 325: 229-234.

14. Liu C, Walter TS, Huang P, Zhang S, Zhu X, et al. (2010) Structural and functional insights of RANKL-RANK interaction and signaling. J Immunol 184: 6910-6919.

15. Anderson DM, Maraskovsky E, Billingsley WL, Dougall WC, Tometsko ME, et al. (1997) A homologue of the TNF receptor and its ligand enhance T-cell growth and dendritic-cell function. Nature 390: 175-179.

16. Lee ZH, Kim HH (2003) Signal transduction by receptor activator of nuclear factor kappa B in osteoclasts. Biochem Biophys Res Commun 305: 211-214.

17. Wada T, McKee MD, Steitz S, Giachelli CM (1999) Calcification of vascular smooth muscle cell cultures: inhibition by osteopontin. Circ Res 84: 166-178.

18. Mohler ER 3rd, Gannon F, Reynolds C, Zimmerman R, Keane MG, Kaplan FS (2001) Bone formation and inflammation in cardiac valves. Circulation 103(11):1522-8.

19. Heymann MF, Herisson F, Davaine JM, Charrier C, Battaglia S, Passuti N, Lambert G, Gouëffic Y, Heymann D (2012) Role of the OPG/RANK/RANKL triad in calcifications of the atheromatous plaques: comparison between carotid and femoral beds. Cytokine 58:300-306

20. Steinmetz M, Skowasch D, Wernert N, Welsch U, Preusse CJ, Welz A, Nickenig G, Bauriedel G (2008) Differential profile of the OPG/RANKL/RANK-system in degenerative aortic native and bioprosthetic valves. J Heart Valve Dis 17:187-193.

21. Simpson CL, Lindley S, Eisenberg C, Basalyga DM, Starcher BC, et al. (2007) Toward cell therapy for vascular calcification: osteoclast-mediated demineralization of calcified elastin. Cardiovasc Pathol 16: 29-37.

22. Nakamura T, Imai Y, Matsumoto T, Sato S, Takeuchi K, Igarashi K, Harada Y, Azuma Y, Krust A, Yamamoto Y, Nishina H, Takeda S, Takayanagi H, Metzger D, Kanno J, Takaoka K, Martin TJ, Chambon P, Kato S (2007) Estrogen prevents bone loss via estrogen receptor alpha and induction of Fas ligand in osteoclasts. Cell 130(5):811-23.

23. Teitelbaum SL (2006) Osteoclasts; culprits in inflammatory osteolysis. Arthritis Res Ther 8(1): 201.

24. Blau CA, Peterson KR, Drachman JG, Spencer DM (1997) A proliferation switch for genetically modified cells. Proc Natl Acad Sci U S A 94: 3076-3081.

25. Jin L, Asano H, Blau CA (1998) Stimulating cell proliferation through the pharmacologic activation of c-kit. Blood 91: 890-897.

26. Weinreich MA, Lintmaer I, Wang L, Liggitt HD, Harkey MA, et al. (2006) Growth factor receptors as regulators of hematopoiesis. Blood 108: 3713-3721.

27. Zeng H, Masuko M, Jin L, Neff T, Otto KG, et al. (2001) Receptor specificity in the self-renewal and differentiation of primary multipotential hemopoietic cells. Blood 98: 328-334.

28. Tey SK, Dotti G, Rooney CM, Heslop HE, Brenner MK (2007) Inducible caspase 9 suicide gene to improve the safety of allodepleted T cells after haploidentical stem cell transplantation. Biol Blood Marrow Transplant 13: 913-924.

29. Spencer DM, Wandless TJ, Schreiber SL, Crabtree GR (1993) Controlling signal transduction with synthetic ligands. Science 262: 1019-1024.

30. Neff T, Blau CA (2001) Pharmacologically regulated cell therapy. Blood 97: 2535-2540.

31. Whitney ML, Otto KG, Blau CA, Reinecke H, Murry CE (2001) Control of myoblast proliferation with a synthetic ligand. J Biol Chem 276: 41191-41196.

32. Collin-Osdoby P, Osdoby P. (2012) RANKL-Mediated Osteoclast Formation from Murine RAW 264.7 cells. Bone Research Protocols 2nd Edition 187-202.

33. Hsu H, Lacey DL, Dunstan CR, Solovyev I, Colombero A, et al. (1999) The TNFR related protein RANK is the osteoclast differentiation and activation receptor for osteoprotegerin ligand. Proc Natl Acad Sci 96: 3540-3545.

34. Rementer CW, Wu M, Buranaphatthana W, Yang HY, Scatena M, Giachelli CM. An inducible, ligand-independent receptor activator of NF-κB gene to control osteoclast differentiation from monocytic precursors. PLoS One. 2013 Dec 27;8(12):e84465.

35. Janckila AJ, Takahashi K, Sun SZ, Yam LT (2001) Naphthol-ASBI phosphate as a preferred substrate for tartrate-resistant acid phosphatase isoform 5b. J Bone Miner Res 16: 788-793.

36. Boyle WJ, Simonet WS, Lacey DL (2003) Osteoclast differentiation and activation. Nature 423: 337-342.

37. Blair HC, Robinson LJ, Zaidi M (2005) Osteoclast signalling pathways. Biochem Biophys Res Commun 328: 728-738.

38. Pohjolainen V, Taskinen P, Soini Y, Rysä J, Ilves M, et al. (2008) Noncollagenous bone matrix proteins as a part of calcific aortic valve disease regulation. Hum Pathol 39: 1695-1701.

39. Ramirez DM, Ramirez MR, Reginato AM, Medici D. Molecular and cellular mechanisms of heterotopic ossification. Histol Histopathol. 2014, 1281-1285.

40. Bevevino AJ, Lehman RA Jr, Tintle SM, Kang DG, Dworak TC, Potter BK. Incidence and morbidity of concomitant spine fractures in combat-related amputees. Spine J. 2014, 646-50.

41. Rumpler M, Würger T, Roschger P, Zwettler E, Sturmlechner I, Altmann P, Fratzl P, Rogers MJ, Klaushofer K. Osteoclasts on Bone and Dentin In Vitro: Mechanism of Trail Formation and Comparison of Resorption Behavior. Calcif Tissue Int. 2013; 93(6): 526–539.

42. Soysa NS, Alles N, Aoki K, Ohya K. Three-dimensional characterization of osteoclast bone-resorbing activity in the resorption lacunae. J Med Dent Sci. 2009 Sep;56(3):107-12.

43. Kleinhans, Schmid FF, Schmid FV, Kluger PJ. Comparison of osteoclastogenesis and resorption activity of human osteoclasts on tissue culture polystyrene and on natural extracellular bone matrix in 2D and 3D. J Biotechnol. 2015 July;205:101–110.

44. Eisenstein NM, Cox SC, Williams RL, Stapley SA, Grover LM. Bedside, Benchtop, and Bioengineering: Physicochemical Imaging Techniques in Biomineralization. Adv Healthc Mater. 2016 Mar 9;5(5):507-28.

45. Speer MY, Chien YC, Quan M, Yang HY, Vali H, McKee MD, Giachelli CM. Smooth muscle cells deficient in osteopontin have enhanced susceptibility to calcification in vitro. Cardiovasc Res. 2005 May 1;66(2):324-33.

46. Ohri R, Tung E, Rajachar R, Giachelli CM. Mitigation of ectopic calcification in osteopontin-deficient mice by exogenous osteopontin. Calcif Tissue Int. 2005 Apr;76(4):307-15. Epub 2005 Apr 11.

47. Osathanon T, Linnes ML, Rajachar RM, Ratner BD, Somerman MJ, et al. (2008) Microporous nanofibrous fibrin-based scaffolds for bone tissue engineering. Biomaterials 29: 4091-4099.

48. Ausk BJ, Gross TS, Bain SD. Botulinum Toxin-induced Muscle Paralysis Inhibits Heterotopic Bone Formation. Clin Orthop Relat Res. 2015 Sep;473(9):2825-30.

49. Koutsopoulos S, Paschalakis PC, Dalas E. The Calcification of Elastin in vitro. Langmuir. 1994, 2423–2428

50. Koutsopoulos S, Dalas E. The Calcification of Fibrin in vitro. Journal of Crystal Growth. 2000, 450–458

51. Koutsoukosa PG, Nancollasb GH. The mineralization of collagen in vitro. Colloids and Surfaces. 1987, 95–108

52. Rittling SR. Osteopontin in macrophage function. Expert Rev Mol Med. 2011.

53. Contractor T, Babiarz B, Kowalski AJ, Rittling SR, Sørensen ES, Denhardt DT. Osteoclasts resorb protein-free mineral (Osteologic discs) efficiently in the absence of osteopontin. In Vivo. 2005, 335-41.

54. Son A, Kim MS, Jo H, Byun HM, Shin DM. Effects of Inositol 1,4,5-triphosphate on Osteoclast Differentiation in RANKL-induced Osteoclastogenesis. Korean J Physiol Pharmacol. 2012, 31-6.

55. Scatena M, Liaw L, Giachelli CM. Osteopontin: a multifunctional molecule regulating chronic inflammation and vascular disease. Arterioscler Thromb Vasc Biol. 2007 Nov;27(11):2302-9.

56. Steitz SA, Speer MY, McKee MD, Liaw L, Almeida M, Yang H, Giachelli CM. Osteopontin inhibits mineral deposition and promotes regression of ectopic calcification. Am J Pathol. 2002 Dec;161(6):2035-46.

57. Pedersen JA, Swartz MA. Mechanobiology in the third dimension. Ann Biomed Eng. 2005 Nov;33(11):1469-90.

58. Lichtman JW, Conchello JA. Fluorescence microscopy. Nat Methods. 2005 Dec;2(12):910-9.

59. Clift MJ, Rothen-Rutishauser B, Brown DM, Duffin R, Donaldson K, Proudfoot L, Guy K, Stone V (2008) The impact of different nanoparticle surface chemistry and size on uptake and toxicity in a murine macrophage cell line. Toxicol Appl Pharmacol 232(3):418-27.

60. Kaskova ZM, Tsarkova AS, Yampolsky IV. 1001 lights: luciferins, luciferases, their mechanisms of action and applications in chemical analysis, biology and medicine. Chem Soc Rev. 2016 Oct 24;45(21):6048-6077.

61. Wang C, Varshney RR, Wang DA. Therapeutic cell delivery and fate control in hydrogels and hydrogel hybrids. Adv Drug Deliv Rev. 2010 Jun 15;62(7-8):699-710.

62. Sivagurunathan S1, Pagel CN, Loh LH, Wijeyewickrema LC, Pike RN, Mackie EJ (2013) Thrombin inhibits osteoclast differentiation through a non-proteolytic mechanism. J Mol Endocrinol 50(3):347-59.

63. Kan L, Kessler JA. Animal models of typical heterotopic ossification. J Biomed Biotechnol. 2011;2011:309287.

64. Lounev VY, Ramachandran R, Wosczyna MN, Yamamoto M, Maidment AD, Shore EM, Glaser DL, Goldhamer DJ, Kaplan FS. Identification of progenitor cells that contribute to heterotopic skeletogenesis. J Bone Joint Surg Am. 2009 Mar 1;91(3):652-63.

65. Dull T, Zufferey R, Kelly M, Mandel RJ, Nguyen M, et al. (1998) A third-generation lentivirus vector with a conditional packaging system. J Virol 72: 8463-8471.

66. Tiscornia G, Singer O, Verma IM (2006) Production and purification of lentiviral vectors. Nat Protoc 1: 241-245.

67. Collin-Osdoby P, Osdoby P. RANKL-mediated osteoclast formation from murine RAW 264.7 cells. Methods Mol Biol. 2012;816:187-202.

68. Larrivée B, Pollet I, Karsan A (2005) Activation of Vascular Endothelial Growth Factor Receptor-2 in Bone Marrow Leads to Accumulation of Myeloid Cells: Role of Granulocyte-Macrophage Colony-Stimulating Factor1. The Journal of Immunology 175:3015-3024.

69. Andersson PS, Kjellén E, Montán S, Svanberg K, Svanberg S (1987) Autofluorescence of various rodent tissues and human skin tumour samples. Lasers in Medical Science Volume 2, Issue 1, pp 41-49.

70. Hastings CL, Roche ET, Ruiz-Hernandez E, Schenke-Layland K, Walsh CJ, Duffy GP. Drug and cell delivery for cardiac regeneration. Adv Drug Deliv Rev. 2015 Apr;84:85-106.

71. Raschke WC, Baird S, Ralph P, Nakoinz I. Functional macrophage cell lines transformed by Abelson leukemia virus. Cell. 1978 Sep;15(1):261-7.

72. Jeon OH, Panicker LM, Lu Q, Chae JJ, Feldman RA, Elisseeff JH. Human iPSC-derived osteoblasts and osteoclasts together promote bone regeneration in 3D biomaterials. Sci Rep. 2016 May 26;6:26761.

73. Kanehisa J, Heersche JN. Osteoclastic bone resorption: in vitro analysis of the rate of resorption and migration of individual osteoclasts. Bone. 1988;9(2):73-9.

APPENDIX

Raw microCT Data: Acid Decalcification (Figure 3.3)

Digestion Time	Pre-Scan BV	Post-Scan BV
5 s	2.298	2.2834
	2.3002	2.2917
10 s	2.2489	2.2273
	1.8195	1.8001
30 s	2.0499	2.0197
	1.9523	1.9259
1 min	1.843	1.7952
	1.588	1.544
5 min	1.9819	1.7684
	1.9206	1.7236
15 min	1.8135	1.3358
	2.0241	1.4553
1 h	2.0046	1.1255
	1.7653	0.8644
24 h	1.8055	0
	1.9491	0.0006

Raw microCT Data: 12 Day Experiment (Figure 3.5)

	Pre-Scan BV	Post-Scan BV
Control	2.1894	2.3617
	2.342	2.4935
	2.4612	2.6068
RAW264.7+iRANK	2.538	2.5568
	2.2553	2.2747
	2.3099	2.332
RAW264.7+iRANK + CID	2.4171	2.4144
	2.3395	2.3096
	2.3358	2.325
	2.2814	2.2671
	2.5145	2.4859

Raw microCT Data: Repeated Cell Seeding Experiment (Figure 3.6)

	Pre-Scan BV	Post-Scan BV
2 Seedings	2.0368	1.9816
	1.8936	1.8099
	2.2138	2.149
	1.8174	1.6767
	1.8635	1.7832
	1.8763	1.834
	2.1382	2.0844
1 Seeding	2.3891	2.3408
	2.1486	2.1002
	1.893	1.8772
	1.8426	1.8195
	2.2122	2.1623
	1.7279	1.6932
Cells Alone	2.2171	2.2793
	2.4087	2.4745
	2.2456	2.2842
	2.4244	2.4656

Raw microCT Data: Human HO Experiment (Figure 3.7)

	Pre-Scan BV	Post-Scan BV
Control (Media Alone)	15.2458	15.307
	16.6059	16.7043
	10.9649	11.1433
	12.3004	12.5393
	12.4823	12.6081
RAW264.7+iRANK Cells	12.6322	12.8189
	9.5672	9.739
	10.6075	10.7476
	11.1824	11.3476
	16.7858	16.9899
RAW264.7+iRANK Cells	9.3832	9.4617
+CID	12.5213	12.606
	11.0297	11.1139
	16.7388	16.849
	13.8096	13.9306
RAW264.7+iRANK Cells	10.4176	10.7938
+CID with OPN Depletion	9.5629	9.7068
	11.3735	11.5544
	8.3018	8.4706
	9.4971	9.6847

Raw microCT Data: Prevention Arm (Figure 4.9)

Bone Volume

Control

Animal ID	Day 14	Day 21	Day 28
uw4580	0.3645	0.2153	0.2021
uw4581	0.0095	0.008	0.0076
uw4582	0.0074	0.0228	0.0302
uw4583	0.0087	0.0195	0.0069
uw4584	1.1652	0.3973	0.3454

Enriched Osteoclasts

Animal ID	Day 14	Day 21	Day 28
uw4590	0.3934	0.3343	0.3083
uw4591	0.6396	0.2476	0.2318
uw4592	0.376	0.3867	0.4079
uw4593	1.2047	0.7875	0.637
uw4594	0.9821	0.7089	0.5539
uw4595	0.756	0.297	0.2854

iRANK Cells

Animal ID	Day 14	Day 21	Day 28
uw4602	1.9086	0.6049	0.5611
uw4603	0.3837	0.4164	0.3696
uw4604	1.7424	0.9713	0.7306
uw4605	1.1867	0.7432	0.709
uw4606	0.5508	0.3154	0.3949
uw4607	0.1853	0.0931	0.0843

Total Volume

Control

Animal ID	Day 28	Day 35	Day 42
uw4585	1.35	1.2942	1.2172
uw4586	0.8056	0.7573	0.6943
uw4587	0.6159	0.8696	0.8492
uw4588	1.4877	1.4283	1.2774
uw4589	1.2902	1.2954	1.1625

Enriched Osteoclasts

Animal ID	Day 28	Day 35	Day 42
uw4596	0.6883	0.6747	0.6184
uw4597	1.4571	1.3536	1.2178
uw4598	1.1361	1.0417	1.0641
uw4599	1.1938	1.1771	1.0652
uw4600	1.017	1.1634	1.0992
uw4601	1.1379	0.7713	0.7534

iRANK Cells

Animal ID	Day 28	Day 35	Day 42
uw4608	0.9236	0.7157	0.6154
uw4609	1.4559	1.2839	1.2268
uw4610	1.4372	1.0908	0.9537
uw4611	1.1756	1.0821	1.0113
uw4612	0.8522	0.7143	0.6485
uw4613	1.6352	1.3657	1.1954

Raw microCT Data: Regression Arm (Figure 4.10)

Bone Volume

Control

Animal ID	Day 28	Day 35	Day 42
uw4585	0.7418	0.7405	0.711
uw4586	0.4901	0.4933	0.463
uw4587	0.3227	0.4888	0.4775
uw4588	0.7736	0.7204	0.6316
uw4589	0.6882	0.7631	0.6755

Enriched Osteoclasts

Animal ID	Day 28	Day 35	Day 42
uw4596	0.4361	0.4605	0.4328
uw4597	0.6787	0.733	0.7016
uw4598	0.8045	0.7725	0.8021
uw4599	0.6831	0.7117	0.6757
uw4600	0.6094	0.7292	0.7321
uw4601	0.7216	0.5977	0.5929

iRANK Cells

Animal ID	Day 28	Day 35	Day 42
uw4608	0.4968	0.4505	0.3938
uw4609	0.8769	0.8197	0.8091
uw4610	0.6206	0.5725	0.5396
uw4611	0.6249	0.5996	0.5828
uw4612	0.4396	0.4021	0.3853
uw4613	0.9861	0.9166	0.8724

Total Volume

Control

Animal ID	Day 28	Day 35	Day 42
uw4585	1.35	1.2942	1.2172
uw4586	0.8056	0.7573	0.6943
uw4587	0.6159	0.8696	0.8492
uw4588	1.4877	1.4283	1.2774
uw4589	1.2902	1.2954	1.1625

Enriched Osteoclasts

Animal ID	Day 28	Day 35	Day 42
uw4596	0.6883	0.6747	0.6184
uw4597	1.4571	1.3536	1.2178
uw4598	1.1361	1.0417	1.0641
uw4599	1.1938	1.1771	1.0652
uw4600	1.017	1.1634	1.0992
uw4601	1.1379	0.7713	0.7534

iRANK Cells

Animal ID	Day 28	Day 35	Day 42
uw4608	0.9236	0.7157	0.6154
uw4609	1.4559	1.2839	1.2268
uw4610	1.4372	1.0908	0.9537
uw4611	1.1756	1.0821	1.0113
uw4612	0.8522	0.7143	0.6485
uw4613	1.6352	1.3657	1.1954